MASTER THESIS

Master Course in Aerospace Engineering

Aeromechanics and Systems

POLITECNICO DI TORINO

Innovative optical sensors for prognostic techniques in the aerospace field: design and development of a test bench for studying the frequency response of FBG sensors.

Supervisor
Prof. Paolo Maggiore
Co-Supervisor
Ing. Matteo Dalla Vedova

Candidate
Giuseppe Spampinato

27 March 2019

Abstract

The thesis work was conducted in collaboration with the interdepartmental center Photonext at the Istituto Superiore Mario Boella (ISMB) and the Department of Mechanical and Aerospace Engineering (DIMEAS) of the Politecnico di Torino. Our Photonext departmental team focuses on the study of innovative optical sensors for prognostic and diagnostic activities in aerospace applications. The purpose of study and experimentation is represented by the FBG (Fiber Bragg Grating) sensor, one of the most popular solutions for optical fiber sensors. These sensors are used to measure physical properties such as vibration, strain, pressure and temperature. They allow to overcome many problems related to the use of traditional sensors through the use of optics as a substitute to electricity. Moreover, thanks to their small size, they can be inserted and used in applications that are impossible for other types of sensors.

This thesis work is focused on an early dynamic analysis of the FBG sensor. For this purpose it was necessary to develop a test bench that considered the conclusions of previous working groups. Several dynamic tests were conducted on the optical fiber, in which only one FBG was inscribed, in order to characterize the frequency response.

Sommario

Il lavoro di tesi qui presentato è stato realizzato in collaborazione con il centro interdipartimentale Photonext presso l'Istituto Superiore Mario Boella (ISMB) e il Dipartimento di Ingegneria Meccanica e Aerospaziale (DIMEAS) del Politecnico di Torino. Il nostro team dipartimentale di Photonext si occupa dello studio di sensori ottici innovativi per attività prognostiche e diagnostiche in applicazioni aerospaziali. L'oggetto di studio e sperimentazione è rappresentato dal sensore FBG (Fiber Bragg Grating), una delle soluzioni più diffuse tra i sensori a fibra ottica. Tali sensori, impiegati per misurare proprietà fisiche come la vibrazione, la deformazione, la pressione e la temperatura, consentono di superare numerosi problemi legati all'impiego dei sensori tradizionali mediante l'utilizzo dell'ottica in sostituzione all'elettricità. Grazie alle loro ridotte dimensioni, inoltre, essi possono essere inseriti ed utilizzati in ambiti applicativi impossibili per altre tipologie di sensori.

Questo lavoro di tesi è focalizzato su una prima analisi dinamica del sensore FBG. Per tale scopo è stato necessario sviluppare un banco prova che ha tenuto in considerazione le conclusioni dei precedenti gruppi di lavoro. Sono stati condotti diversi test dinamici sulla fibra ottica, in cui era fotoinciso un solo FBG, con il fine di effettuarne la caratterizzazione della risposta in frequenza.

Contents

List of Figures

List of Tables

Chapter 1

Introduction

In the last 25 years, the development of the optical fiber has undergone considerable growth. Since the mid-1990s, it has been used in the field of telecommunications as information-carrying. Today, light wave communication systems have become the preferred method to transmit large amounts of data and information from one point to another. The optical fiber has interesting advantages such as low losses, no problems of electromagnetic interference (EMI), small in dimension, light in weight, safe, low cost and maintenance [9]. Optical fiber is used as a sensor for structures, systems and devices. Fiber sensors rely on the proprieties of the optical fiber to convert an environmental effect into a modulation of the light beam passing through it, with change of phase, frequency, intensity or polarization state [3]. They are passive components that do not need electric energy to work. In addition, they enable multiplexing signals, so it is possible to control and operate many sensors. Fiber optical sensors (FOS) appeared just after the invention of the practical optical fiber by Corning Glass Works in 1970, now Corning Incorporated, that produced the first fiber with losses below 20 dB/km [7]. Technological advances in fiber production have led to attenuation in the order of 0.2 dB / km. In recent years particular attention has been directed to Fiber Bragg Grating sensors for different applications. The reduction of production costs and containment of operating costs have led to the use of this technology in various engineering sectors. Today, in the aerospace field, network of fiber optic sensors are used in ground tests, design and also in some aircraft in services. The use of these sensors guarantee weight savings, safety, diagnosis and prognosis in real time of structural health and on-board systems that are difficult to access during maintenance inspections. The long term vision is that all new aircraft will fly with Fiber Bragg Grating (FBG) optical sensors.

1.1 Thesis description

This thesis work is focused on an early dynamic analysis of the FBG sensor. In the initial phase, a test bench was set up where the tests were conducted. Some necessary components have been designed by CAD software and made in aluminium and others in PLA. In the second part of the work, the use of the piezoelectric actuator with its control software were studied. Then, Matlab scripts were written to allow data processing. The first tests conducted were necessary to optimize the matlab programs and the data acquisition and processing operations. In the third part, tests were carried out on the optical fiber and its frequency response was analysed. Finally, the data provided by the PZT actuator were validated using an accelerometer.

The presentation of the thesis work was divided as follows:

- Chapter 2: *Optical Fiber.*
  This chapter refers to the optical fiber. There is a brief description with reference to the materials and types of optical fiber. In the section 2.3, there is an explanation of the optical phenomenon on the propagation of light in the fiber, in particular the Snell's theory. Lastly, the main advantages in the use of optical fibers are shown.

- Chapter 3: *Fiber Optic Sensor.*
  This chapter introduces the use of the optical fiber in the sensing and monitoring systems. The Bragg grating sensor is presented in detail, showing the fundamental equations and the principle of operation. In addition, the main advantages of using the fiber optic sensing systems, in particular the FBG sensor are highlighted.

- Chapter 4: *Test Bench setup*
  This chapter shows the setup of the developed test bench. The setup used is similar to the previous works, to which necessary modifications have been made. Each hardware and device component is described, in particular the two main tools used for the tests: the SmartScan interrogator and the Modular piezo controller. In the Cad Design section the components designed for mounting the PZT actuator and micropositioner on the breadboard are shown and in addition the components needed for gluing the optical fiber. Finally, the locking system of the optical fiber used for the tests is illustrated.

- Chapter 5: *Softwares for the tests.*
  Two softwares are required to perform the tests. The first is the *PIMikroMove*. This software allows the parameter of the PZT actuator to be controlled and sends commands to this device. Specifically, *PI Wave Generator Tool* is used to create a sinusoidal command. The second software is *SmartSoftSSI.* This is the graphical interface of SmartScan interrogator for data acquisition of the FBGs sensors.

For post-processing, Matlab scripts have been written that allow the analysis of the data obtained from the tests.

- Chapter 6: *Tests and measurements.*
  This chapter shows the tests carried out and the results obtained. Several tests have been performed. The results and relative conclusions are discussed for each test. In the chapter, the problems and limitations identified are highlighted. The last section shows the use of an accelerometer to validate the operation of the piezoactuator.

- Chapter 7: *Conclusions and future works.*
  In the conclusions, possible future thesis works to continue this study are presented. In particular, to overcome the problems encountered in order to obtain a complete characterization of the FBG sensor.

Chapter 2

Optical Fiber

2.1 Description of Optical Fiber

Optical fibers are filaments of glassy or polymeric materials that allow light to be carried inside them. They are composed primarily of silicon dioxide (SiO_2), though minute amounts of other chemicals are often added. The fiber consists of three concentric layers:

- core
- cladding
- coating.

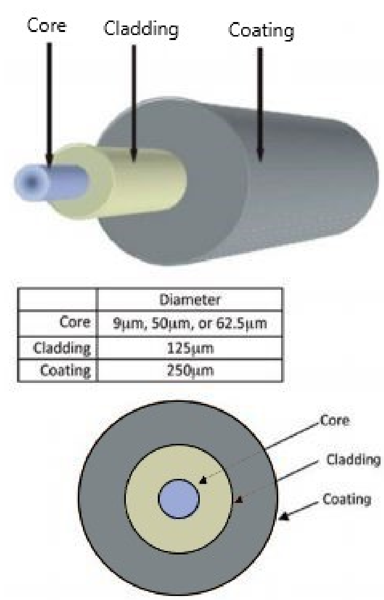

	Diameter
Core	9µm, 50µm, or 62.5µm
Cladding	125µm
Coating	250µm

Figure 2.1: Structure of optical fiber

As shown in the figure 2.1, the core is the inner layer where light is transmitted. A single-mode fiber has a diameter of 9 microns whereas a multi-mode fiber measures 50-62.5 microns . The index of refraction is high in the core while it is lower in the cladding. This layer has a diameter of 125 microns and keeps the light inside the core due to the effect of reflection. The coating is made of polymeric material with a diameter of 200-250 microns and it is used to isolate the inner layers from the external environment.

The materials for the optical fiber are chosen based on the degree of transparency and they must have a low optical loss with a specific index of refraction. The glass fiber (SiO_2) is doped with small amounts of others elements to modify physical and optical properties. These elements are called dopant and allow to increase or decrease refractive index of silica. For this reason P_2O_5 or GeO_2 are suitable for the fiber core characterized by a high refractive index, while B_2O_3 or F are used for the cladding with a very low refractive index. The main methods of manufacturing fibers are Plasma CVD, Modified chemical vapor deposition (MCVD), Outside vapor deposition (OVD) and Vapor-phase axial deposition (VAD) [4].

2.2 Types of optical fiber

The light propagates within the fiber according to electromagnetic waves having different paths and geometries known as propagation modes. As shown in the figure 2.2, three types of fibers can be obtained based on the propagation modes:

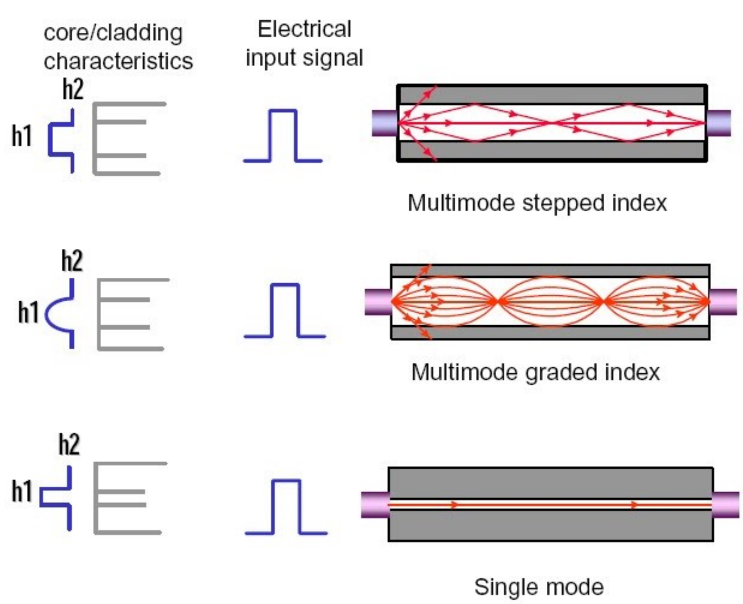

Figure 2.2: Fiber classification

- Step-index multimode fiber has a large core diameter with a uniform index of refraction. In this type of fiber can have many propagation modes. The cladding has a refractive index slightly lower than core. The name step-index is given by refractive index discontinuity between the core and the cladding. The large core size is relatively easy to work and it is used in applications that require high bandwidth over relatively short distances. Other characteristics are the low coupling losses. It can be used with both LED and laser sources, and data rates are lower due to modal dispersion [8].

- Step-index single mode fiber is an optical fiber in which only one mode propagates. The light beam passes through the fiber without reflections and the modal dispersion is eliminated. The bandwidth is limited by modal dispersion so for this reason the single mode fiber has a higher bandwidth than the multimode. This type of fiber is used for long distances applications in which low signal loss and high data rates are required. Step-index single mode fiber optic can be used only with laser sources.

- Graded-index fiber has a core with diameter wider than the single-mode fiber. A large number of modes are propagated in the fiber. The properties of this fiber are a compromise between the single mode and multimode feature. The refractive index decreases parabolically from the core center toward the cladding, therefore the light travels at the edge of the core rather than in the center. The modal dispersion is reduced because the modes travel times are nearly equal. Graded-index fiber has bandwidths which are greater than the step-index fiber, but still much lower than single-mode fiber. This fiber is used for medium range applications.

2.3 Fundamental theory of optical fiber

The propagation of light within the fiber is based on the theories of the geometric optics. The phenomenon that allows the signal to be transmitted through the optical fiber is known as Total Internal Reflection (TIR). The light, passing from one transparent medium to another with different refractive index, undergoes the phenomenon of refraction according to the Snell's law:

$$n_1 sin\theta_i = n_2 sin\theta_r \tag{2.1}$$

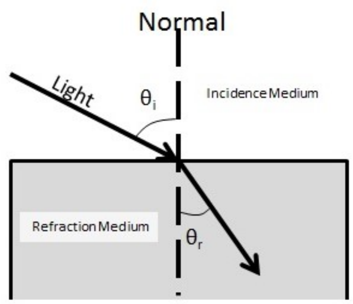

Figure 2.3: Snell's law

where $n_1$and n_2 are the medium refractive index while θ_i is the angle of incidence and θ_r is the angle of refraction.This happens in optical fibers where the light passes from the core with greater refractive index to the cladding with lower refractive index. There is a limit angle $\theta_i = \theta_{cr}$ beyond which the radiation is totally reflected:

$$sin\theta_{cr} = \frac{n_1}{n_2} \tag{2.2}$$

from this equation we obtain the critical angle when $\theta_2 = 90°$. Total internal reflection is obtained when the incidence angle is greater than or equal to the critical angle θ_{cr}. For total reflection internal to occur the angle of incidence formed by the direction of an external ray with the fiber axis must be less than a maximum angle α_{max}. This angle can be obtained by Snell's law by referring to figure 2.4 :

$$n_0 sin\alpha = n_1 sin\left(\frac{\pi}{2} - \theta_c\right) \tag{2.3}$$

$$n_1 sin\theta_c = n_2 sin\left(\frac{\pi}{2}\right) \tag{2.4}$$

replacing θ_c in the equation 2.3 you get it

$$sin\alpha_{max} = \frac{n_1 cos\theta_c}{n_0} = \frac{\left(n_1^2 - n_2^2\right)^{1/2}}{n_0} \tag{2.5}$$

where $\left(n_1^2 - n_2^2\right)^{1/2} = NA$ numerical aperture. So the maximum external incidence angle called acceptance angle is defined as

$$\alpha_{max} = arcsin\left(\frac{NA}{n_0}\right) \tag{2.6}$$

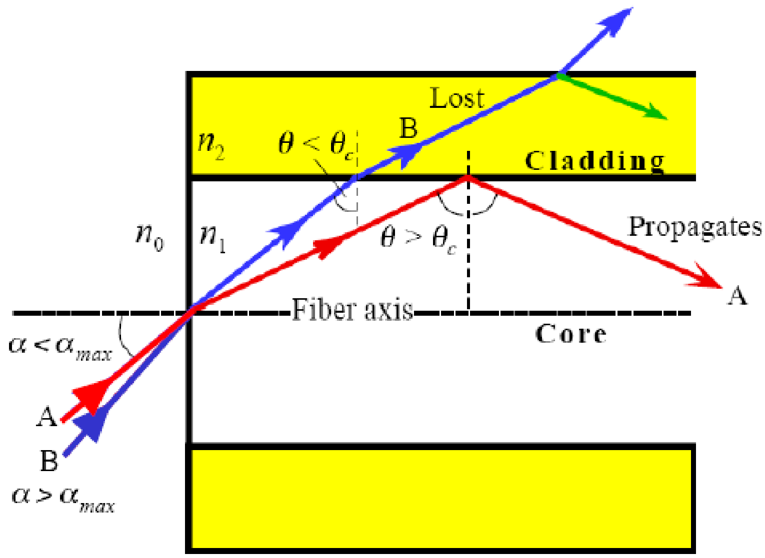

Figure 2.4: Snell's law applied to optical fiber

The set of possible incidence trajectories having an angle less than or equal to the acceptance angle, constitutes the acceptance cone.

2.4 Advantages and disadvantages of the fiber optic systems

The main advantages of the optical fibers have emerged in the telecommunications sectors. The fiber optic systems allow to have better performances than the coaxial copper cable, microwave systems and wide-band radio. Many of these advantages are particularly important for aerospace applications:

- The fiber optic has a bandwidth such as to allow the transport of large amounts of information over long distances with low signal losses (0.2 dB/km [5]). Coaxial cables have a typical bandwidth parameter of a few MHz/km, whereas fiber optic cables have a bandwidth in the region of 400 MHz/km[2].

- The fiber optic cables are manufactured using non-conducting materials such as glass and plastic. The signal that passes through the fiber is immune to radio-frequency interference (RFI) and electromagnetic interference (EMI). For this reason, in many applications, optical fiber is preferable compared to metallic cables particularly for reliable monitoring and telemetry [5].

- The fiber is extremely insulating and doesn't allow interference and coupling with other communication channels. This leads to a higher degree of data security

- The realization of fiber optic systems have a lower cost than systems that use metallic cable. The optical fiber are relatively inexpensive and easy to manufacture. Over the years, with new technology, the costs of production, transport and installation have decreased. Moreover the fiber optic systems needs little maintenance.
- The optical fiber is light and flexible. It is resistant to high temperatures, to corrosion and can be used in a harsh environment. There is no risk of sparking as happens with metallic cables.

The use of optical fiber also has disadvantages including:

- The use and maintenance of optical fibers are not economical because it is necessary to use many expensive equipment. Using FBG sensors requires an expensive interrogation system, also requires expensive equipment to splice two or more optical fibers.
- The optical fibers have to be installed without high curve radius because of the increase optical losses.
- Optical fiber is very delicate for its thinness. If it is not well protected it is subject to mechanical damage.

Chapter 3

Fiber Optic Sensor

3.1 Introduction to fiber optic sensors

The use of optical fiber as sensor was initially thought for Structure Health Monitoring (SMH). The fiber optical sensors (FOS) allow to evaluate continuously and in real-time the structural characteristics and their degradation therefore to realize so-called “Smart Structure”. The importance of structure monitoring doesn’t only concern the civil field but several engineering applications. In the aerospace field, with the introduction of new composite material, the activity of sensing and monitoring has become important. Sensors are used in the design and testing phase to knowledge the behaviour, to detect defect and to estimate operative life time of structures in composite material [11]. In aircraft, other than airframe, the FOSs can be used in all on-board systems. The advantage of immunity to electromagnetic interference is very considerable. On account of the increase of electronic instrumentation on-board, the use of fiber optic sensors have become very important on “more electric aircraft” because they are immune to electromagnetic interference in addition to their small size and light weight. The purpose is to improve the reliability, efficiency, safety and decrease inspection and maintenance operation times.

3.2 Optical Fiber Sensing System

The main elements of an optical fiber sensing system are the following:

- Fiber optics
- Light sources: LED or LASER
- Transducer or sensing elements

- Detector

The light signal sent by the source is modified by changing some parameters as frequency, phase, polarization state and intensity. The signal is modulated by the transducer and sent to the detector, that detects the output of the sensor. The fiber optic sensors can be divided into two main categories: direct (intrinsic) and indirect (extrinsic).

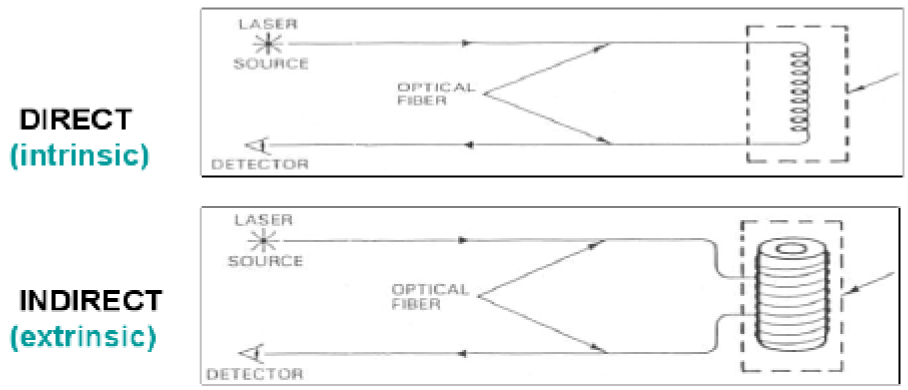

Figure 3.1: Schematic configurations of FOS

- Intrinsic sensors: the fiber itself is the transducer. The sensing elements is included in the fiber. An internal device is used for light signal modulation and the backreflecting part of it [12]. Fiber Bragg Grating (FBG) is a typical direct sensor. This sensor are explained in the next section. FBGs sensors are the subject of this thesis.

- Extrinsic sensors use the optical fiber only to propagate the light. The modulation is performed by some external transducers.

There are other categories of fiber optical sensors, for example multiplexed sensors, multiparameter sensors, distributed sensors and semidistributed sensors. Fiber grating sensors can have several configurations which are part of these categories.

What distinguishes the FOS from other technologies is the possibility to use a single fiber to host a plurality of sensing points, and detecting multiple parameters in the same fiber [12].

3.3 Fiber Bragg Gratings Sensors

Optical fiber Bragg grating technology has its origins in the discovery of the photosensitivity in optical fibers. FBGs sensors are used for many applications. In the civil field they are very useful for to monitoring dams, bridges, highways, buildings, etc. They are also employed, also, for non destructive testing, remote sensing and smart structure in several engineering sectors. In the mechanical and aerospace field, FBGs are used to measure physical properties, for instance: vibration, strain, pressure and temperature. Advantages of FBGs compared with other sensor technologies are as the follows as reported in [9]:

- direct transformation of the sensed parameter to optical wavelength,
- no resistive heating and non-conductive,
- small size,
- highly multiplexed,
- immune to electromagnetic interference,
- low fiber loss at 1550 nm [9](for remote sensing),
- environmentally more stable.

The Bragg grating is obtained through a periodic variation of the refractive index within the core of optical fiber. It works like as wavelength-selective mirrors for incident light. The Bragg has the function of filtering and allowing to select particular wavelength.

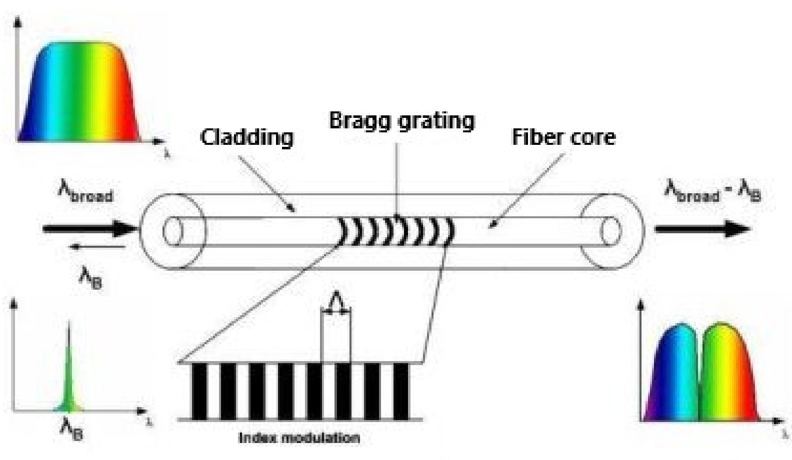

Figure 3.2: Bragg grating principle of operation

As shown in the figure 3.2, when the light crosses the Bragg gratings, part of energy is transmitted through, and another back-reflected. The maximum reflected light signal has a particular wavelength called *Bragg wavelength, λ_B,* expressible by the following equations:

$$\lambda_B = 2n_{eff}\Lambda \tag{3.1}$$

where n_{eff} is the effective refractive index of the fiber and Λ is the period of the grating. The variation of the Bragg wavelength is due to a change of the refractive index or the periodicity of the Bragg grating. An axial strain, due to an external force, for instance, may change both Λ and n_{eff} , for the photo-elastic effect. These parameters can be altered, also, for thermo-optic effect with thermal dilatation. For this reason, the FBGs are used as a sensors to detect a shift in the wavelength of the reflected light output. In this way you can obtain measurements of strain, displacement, temperature, pressure and vibration. This is monitored as a shift in the wavelength of the reflected light output. The length of the Bragg grating influence the intensity of the response and the FWHM (full-width-halfmaximum) or bandwidth. As the length of the grating increases, the reflected power will be greater. Typically, the FWHM is 0.05 to 0.3 nm in most sensor applications [7].

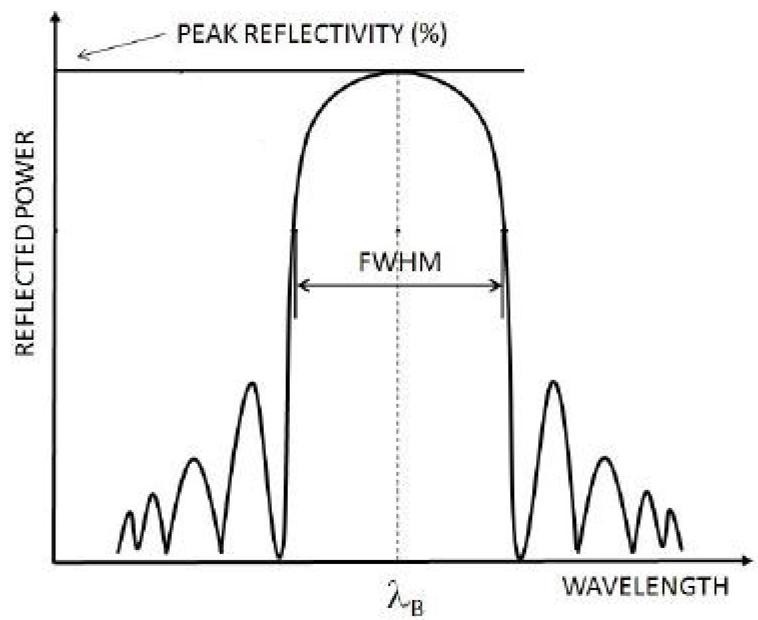

Figure 3.3: Bragg reflection wave shape

3.3.1 Bragg Grating Structure

The structure of the FBG can vary via the refractive index, or the grating period. The grating period can be uniform or graded, and either localized or distributed in a superstructure. The common structures for FBGs are the following:

- **Uniform fiber Bragg gratings**
  The uniform gratings have a modulation of the refractive index constant in amplitude and period.

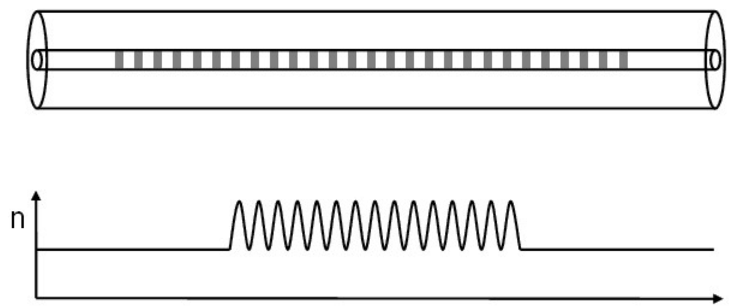

Figure 3.4: Uniform fiber Bragg gratings

- **Apodized gratings**
  The modulation can assume a Gaussian shape or a raised cosine profile with noncostant amplitude.

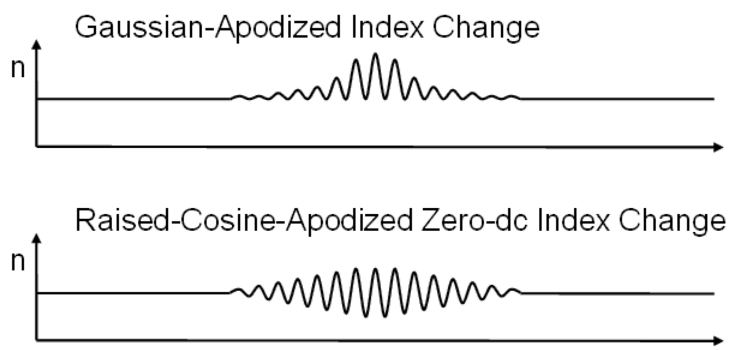

Figure 3.5: Apodized fiber Bragg gratings

- **Chirped fiber Bragg gratings**
  The amplitude of the refractive index modulation is constant, but the period is different in each portion of the grating. With the variation of the period along z, also the Bragg wavelength is function of z.

Figure 3.6: Chirped fiber Bragg gratings

- **Tilted fiber Bragg gratings**
  In a tilted gratings structure, like in a uniform FBG, a modulation of the refractive index with uniform period and amplitude is inscribed into the fiber core. The modulation is not parallel to the fiber propagation plane z. The refractive index modulation is tilted by a θangle. The angle of tilt in a TFBG has an effect on the reflected wavelength, and bandwidth.

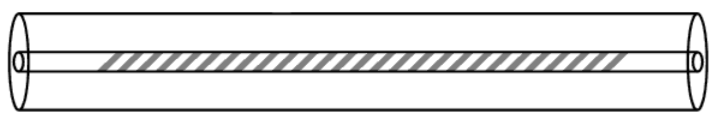

Figure 3.7: Tilted fiber Bragg gratings

- **Phase-shifted fiber Bragg gratings**
  Phase-shifted FBGs contain two identical effective refractive index gratings and a π phase-shifted section.

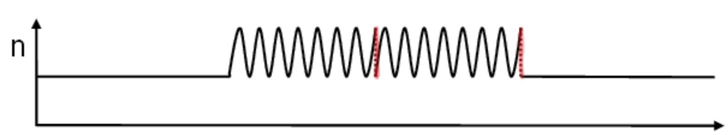

Figure 3.8: Phase-shifted fiber Bragg gratings

According to the length of the grating period (Λ), it is possible to have a *short period Bragg gratings* and *long period Bragg gratings*. In a short period gratings (SPG), the refractive index modulation of the core has a periodicity on the order of 0.5 μm. In contrast, the long-period grating (LPG) has a period typically in the range 100 μm to 1 mm. The optical fiber used for the purposes of this thesis has a short period and uniform Bragg grating.

3.3.2 Elastic-thermo-optic effect

As previously mentioned, temperatures and strain can induce variations in the period of the Bragg grating and the refractive index. Deriving the equation 3.1 with respect to temperature and length we get the following equations:

$$\frac{\Delta\lambda_B}{\Delta T} = \frac{1}{\Lambda}\frac{\partial\Lambda}{\partial T}\lambda_B + \frac{1}{n_{eff}}\frac{\partial n_{eff}}{\partial T}\lambda_B \tag{3.2}$$

or rearranging,

$$\frac{\Delta\lambda_B}{\lambda_B} = \frac{1}{\Lambda}\frac{\partial\Lambda}{\partial T}\Delta T + \frac{1}{n_{eff}}\frac{\partial n_{eff}}{\partial T}\Delta T \tag{3.3}$$

The first term to second member corresponds to the thermal expansion of silica (α) and the second term is the thermo-optic coefficient (η). The equation 3.3 can be rewritten as:

$$\frac{\Delta\lambda_B}{\lambda_B} = (\alpha + \eta)\Delta T \tag{3.4}$$

The partial derivative of 3.1 with respect to displacement:

$$\frac{\Delta\lambda_B}{\lambda_B} = \frac{1}{\Lambda}\frac{\partial\Lambda}{\partial T}\Delta L + \frac{1}{n_{eff}}\frac{\partial n_{eff}}{\partial T}\Delta L \tag{3.5}$$

The first term to second member is the strain of the grating period due to the extension of the fiber. If L is the length of the fiber, $\Delta L/L$ is the relative strain. This strain is the same for the Bragg grating, in fact $\Delta L_{FBG}/L_{FBG} = \Delta L/L$. The second term is the photo-elastic coefficient (ρ_e), the variation of the index of refraction with strain. The form of the Bragg wavelength displacement with strain is due to opposite effect of two terms in the equations 3.5: the first term increases the Bragg wavelength, while the second term induces a decrease of the effective refractive index and thus decreasing the Bragg wavelength. Calling ε_z the longitudinal strain of the grating, the equation 3.5 can be rewritten as:

$$\frac{\Delta\lambda_B}{\lambda_B} = (1 - \rho_e)\varepsilon_z \tag{3.6}$$

Combining the effects of temperature and strain to get the equation for Bragg wavelength sensitivity:

$$\frac{\Delta\lambda_B}{\lambda_B} = (1 - \rho_e)\varepsilon_z + (\alpha + \eta)\Delta T \tag{3.7}$$

or rearranging,

$$\frac{\Delta\lambda_B}{\lambda_B} = K_{\varepsilon_z}\varepsilon_z + K_T\Delta T \tag{3.8}$$

where $K_{\varepsilon_z}$and K_T are two proportionality constants. For the purpose of the thesis the effect of the temperature has been neglected. Therefore the strains are calculated as:

$$\varepsilon_z = \frac{1}{K_{\varepsilon_z}} \frac{\Delta\lambda_B}{\lambda_B} \tag{3.9}$$

3.3.3 Methods for fiber Bragg grating fabrication

The production methods of Bragg gratings can be divided into two categories: those that are holographic and those that are non-interferometric. For the production of the Bragg gratings, the germanium-doped fibre is used for its photosensitivity. The photosensitivity allows to change the refractive index of the core of the fiber with exposure to UV radiations. The main methods are described below:

- **Interfering beam method**

  This is the most widely used holographic method for the manufacture of Bragg gratings. A laser source is used. The UV beam is split in two by a beam splitter. The two rays propagate until they reach two orientable mirrors where they are reflected. The two reflected rays to meet again to form a interference pattern over the fiber to be inscribed. Cylindrical lenses concentrate the beams, with reciprocal angle of θ, in the inscribing area of the fiber The refractive index of the fiber changes according to the intensity of light that it is exposed to. The period of the interference pattern Λ depends on the wavelength of the light used for writing λ_{laser} and also on the half-angle between the two interfering beams as shown in 3.10

  $$\Lambda = \frac{\lambda_{laser}}{2\,sin\theta} \tag{3.10}$$

  Bragg wavelength (λ_B) depends on the laser wavelength, and on the intersection half-angle.

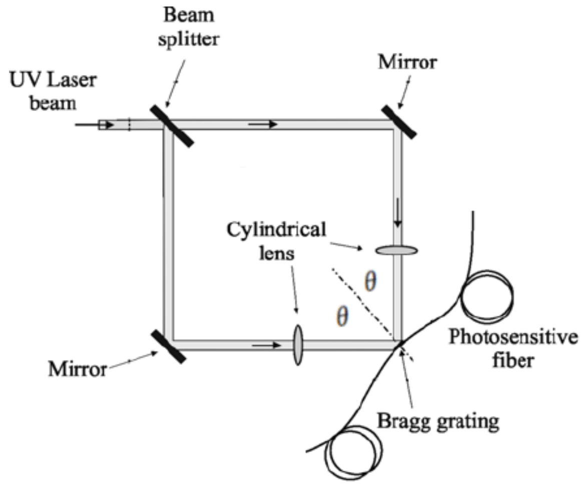

Figure 3.9: Simple setup of interferometer technique

- **Phase mask method**

  For the phase mask technique a diffractive optical element is used that spatially modulates the UV beam with the Λ_{pm} period. A laser beam incident on the phase mask is diffracted into several diffraction orders. Orders +1 and -1 have the most power, while zero order is suppressed to less than 3%. The orders +1/-1 are divergent. In the area of interference pattern, the two orders cross each other with a period:

$$\Lambda = \frac{\Lambda_{pm}}{2} \tag{3.11}$$

  The fiber is placed in contact with or in close proximity to the phase mask [7]. Bragg wavelength (λ_B) depends essentially on the phase mask periodicity.

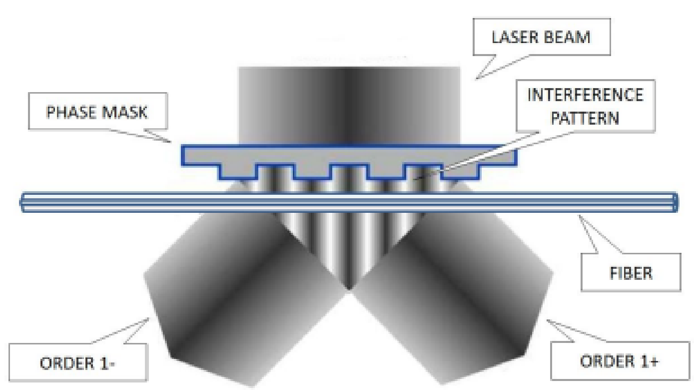

Figure 3.10: Phase-mask technique scheme

- **Point by point**

  This technique uses a highly focused femtosecond laser (FSL) systems. The FSL sends highly energetic and high-precision pulses directly into the optical fiber core. The narrow duration of the pulse ensures that the permanent index change in the core remains confined, whereas the scanning speed determines the Bragg wavelength.

Chapter 4

Test Bench setup

This chapter describes the test bench with its components used to conduct fiber tests. Each individual device is explained in detail. Several components have been designed using *SolidWorks* software and made of PLA and aluminium. These components are used for the locking systems of the optical fiber. The main devices used to perform the tests are the following:

- SmartScan interrogator
- Piezoelectric actuator and control module

The following sections show how they work and how to use them. In the figure 4.1 the complete assembly test bench is shown.

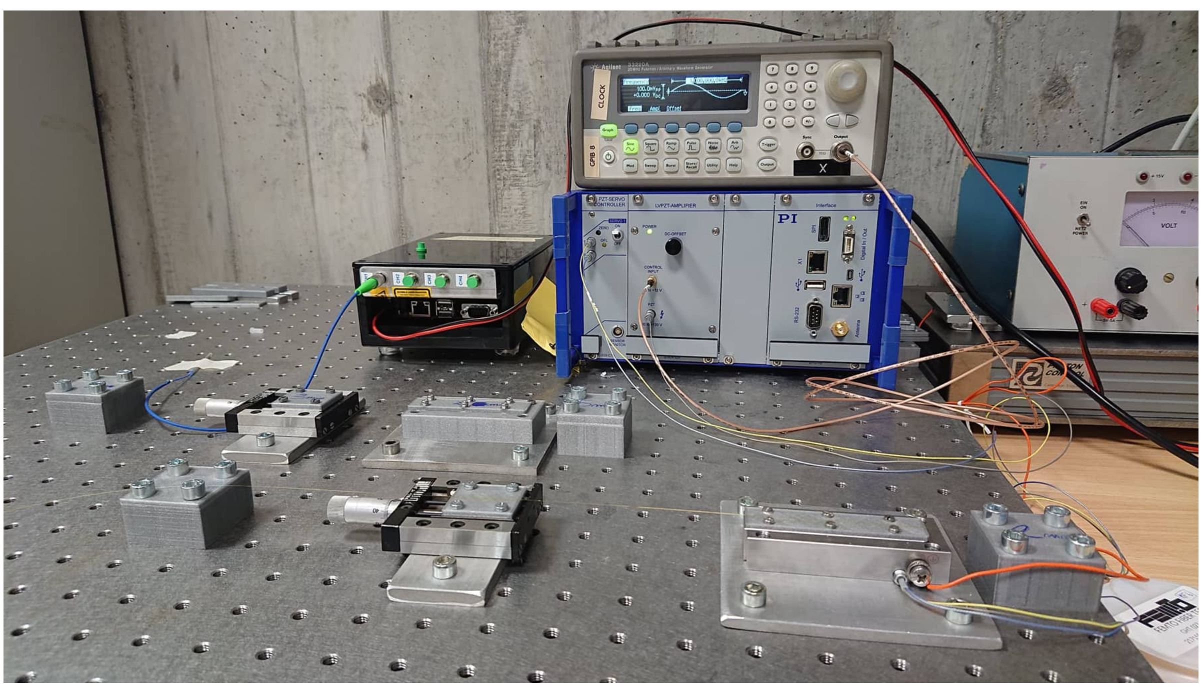

Figure 4.1: Test bench setup

4.1 Optical breadboard

All components have been positioned and fixed on a optical breadboard. The Bragg sensor is susceptible to vibration. In fact, vibrations can cause disturbances on the Bragg wavelength (λ_B) by reducing the measurement accuracy. A 59 mm thick breadboard was used to dampen vibrations. It was verified that only the use of the breadboard was effective for damping. For this reason, the optical table is positioned on the wooden desk. It was not necessary to use an anti-vibration table.

Figure 4.2: The M-PG-33-2-ML Precision Grade Modal Damped Honeycomb Core Optical Breadboard

The Optical breadboard has a 300 mm width, a 600 mm length, and is 59 mm thick with M6-1.0 holes on 25 mm grid. It has a 4.8 mm ferromagnetic steel mounting surface, patented modal damping, sealed holes, steel honeycomb core, and self-damping side panels.

On the breadboard are mounted the piezo actuator, micro translation stages and another locking systems station. The other instruments were simply placed on the breadboard.

4.2 FBG interrogator

The device used for the measurement of reflection and transmission spectra of Bragg gratings is the SmartScan SBI, an optoelectronic unit.

The Bragg wavelength of the reflection peaks shifts when the FBG sensor is strained (fig. 4.3). For measuring strain with FBGs it is necessary to measure these shifts very precisely.

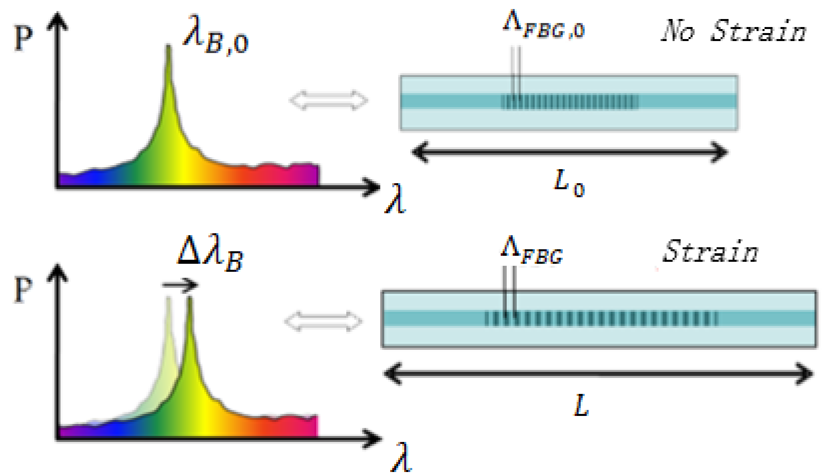

Figure 4.3: Shift of Bragg wavelength applied a strain

The scan generator tunes the light source, sweeping it back and forth across its range such that at any given instant the wavelength of light being transmitted down the optical fibers is known. When this wavelength coincides with the Bragg wavelength of an FBG, light is reflected back down the optical fiber to a photo-detector. The scan generator also supplies a timing signal to the processor, allowing it to convert the intensity vs. time information into a spectrum. Further processing is performed to identify peaks in this spectrum, find their peak positions and convert these to strain or temperature.

SmartScan SBI is a complete FBG interrogator offering dynamic measurement of numerous connected FBG sensors from a single board Eurocard format (fig 4.4). The card has been installed in a box to be usable and protect.

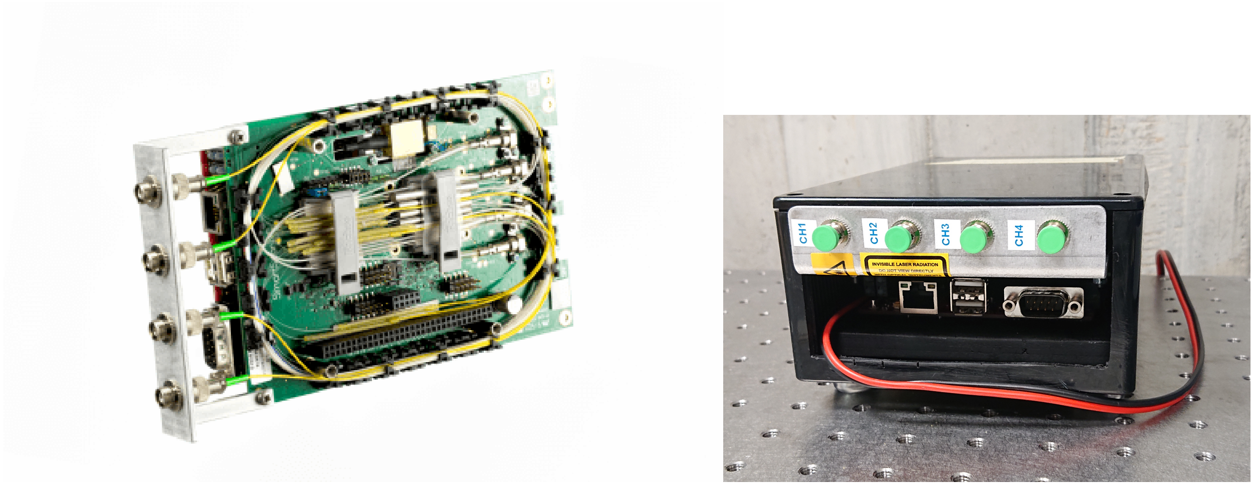

Figure 4.4: SmartScan SBI

This single board instrument has an integrated laser source which allows high frequency and high resolution interrogation. In particular, the frequency interrogation used in the test is $12500 Hz$. This interrogator has four input channel and each channel can process 16 Bragg sensors. The maximum scan frequency is $25 KHz$ for only one sensor. The scan frequency decreases when multiple sensors are connected. SBI is connected to the PC via LAN connection. The data recorded by the interrogator and sent to the PC are processed and stored using the user interface software *SmartSoftSSI*.

4.3 Piezoelectric Actuator

Piezoelectricity is the property of some materials to generate an electric field in response to a mechanical stress applied and vice versa. Piezoelectric actuators use the inverse piezoelectric effect by converting electrical energy (voltage and current) into mechanical energy (forces and displacements).

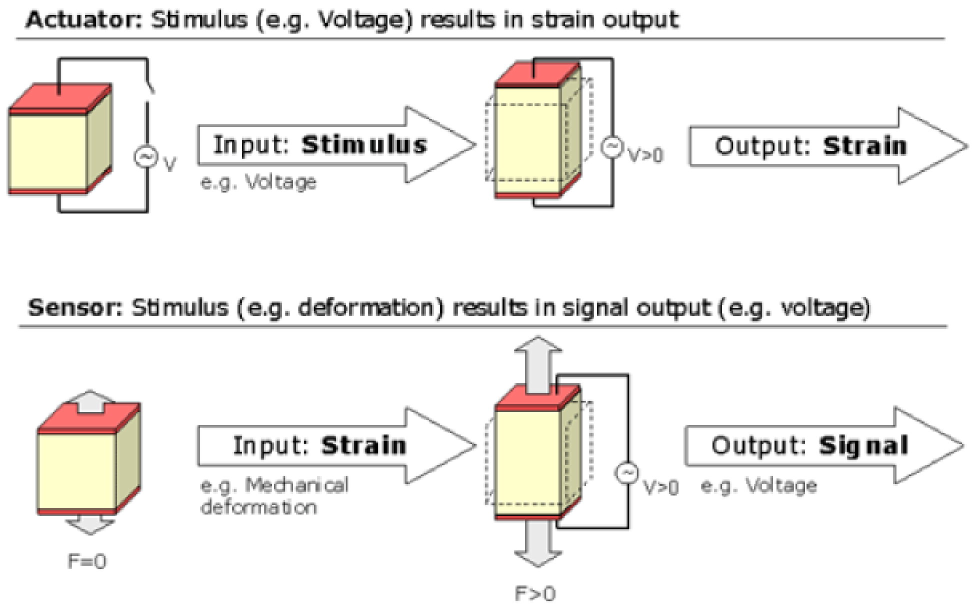

Figure 4.5: Schematic of the piezoelectric effect

Piezoelectric materials generally belong to the class of ferroelectrics. For maximum response, ferroelectric materials must be polarized by applying an electric field to the material, while simultaneously heating. The materials most commonly used are referred to generically as $Pb(Zr,Ti)O_3$ or PZT. PZT ceramics are solid solutions of $PbZrO_3$ and $PbTiO_3$[6].

Piezo technology is a class of actuation that is capable to ultra-precision positioning with nanometer accuracy and short response time. The most common types of actuators are multi-layer actuators (MLA) and bender actuators. A multi-layer piezoelectric actuator consists of a series of piezoelectric plates stacked one above the other and closed between two electrodes. In an MLA actuator the applied voltage causes a deformation in the direction of the electric field lines, orthogonal to the plane of the plate. Individual layers are mechanically connected in series and electrically connected in parallel. MLA are particularly suitable for highly dynamic operation due to their high resonance frequencies. Furthermore, it allows high mechanical performance with response times in the order of microseconds. The longitudinal displacement can be estimated with the following equation:

$$\Delta L_{long} = n d_{33} V \tag{4.1}$$

where

- ΔL_{long} is longitudinal displacement $[m]$,
- n is the number of stacked ceramic layers,

- $d_{33}$is longitudinal piezoelectric large-signal deformation coefficient $[m/V]$,
- and V is the operating voltage $[V]$.

The figure 4.6 shown the *PICMA*® Stack multilayer piezo actuator $P-885.91$.

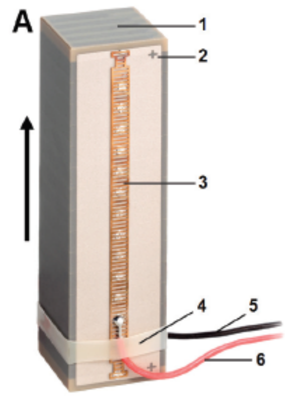

Figure 4.6: *PICMA*® Stack multilayer piezo actuators

The number in the figure 4.6 are respectively:

1. Ceramic end surface (passive PZT ceramic)
2. Marking for positive pole
3. Contact strip
4. Shrink tube (strain relief of the stranded wires)
5. Black stranded wire: Connection for ground (-)
6. Red stranded wire: Voltage connection (+)

The arrows, in the figure 4.6, indicate the expansion direction of the piezo actuator when a positive voltage is applied. The maximum travel range is $38\,\mu m$. Operating voltage range is -20 to $120\,V$ and a resonant frequency of $40\,kHz$.

This piezo actuators is installed in the P-753.31C stage, a high-dynamics piezo nanopositioning system.

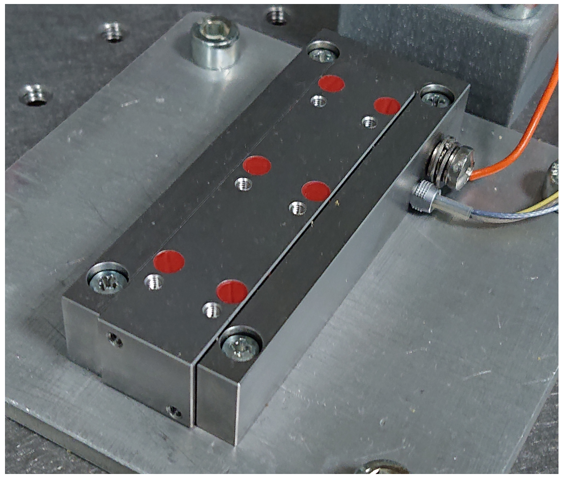

Figure 4.7: P-753.31C produced by Physik Instrumente (PI) GmbH & Co.

It allows dynamic motion by sinusoidal command with closed-loop resolution of $0.2\,nm$. The maximum operating frequency is $1\,KHz$ (without load); this is one third of the resonant frequency. P-753.31C is driven by applied control input voltage. The power supply system and control logic is detailed in the next section.

4.3.1 Modular Piezo Controller

The modular piezo controller consists of three modules for the power supply, the servo controller and the digital interface. The device is E-500 produced by Physik Instrumente (PI) GmbH & Co. This system allows to control a piezo actuator in analog or digital mode. Control takes place either directly at the analog inputs of the amplifiers or via the interface module with digital interfaces.

Figure 4.8: E-500 Modular Piezo Controller

The all modules are installed in the same chassis and communicate automatically over the backplane. The single modules are detailed below.

- **Amplifier Module**

  E-504.00F is the high-power piezo amplifier module. This module supply power to the PZT. The input signal should always be in the range of 0 to $10V$(excursions to -2 or $+12V$ may cause overflow). This control input voltage gives the target (either as voltage or position, depending on the servo mode). The input signal is amplified and the output voltage is -30 to $+130V$. An analog signal generator (e.g. frequency generator) can be connected to the control input port for the analog operation. The input signal is processed by the Servo-Controller module before amplification. Furthermore only in analog mode, DC-offset potentiometer adds 0 to $10V$ to the control input signal.

- **Servo-Controller Module**

  E-509.C1A is a displacement sensor and position servo-control module for PZT actuators. This module allows to control the position (displacement) of piezoelectric actuators with nanometer resolution. The control signal generated in either analog or digital mode is processed by a small add-on printed circuit board (PCB, E-802.55 Servo-Control Submodule). The position control occurs through servo-loop algorithm. The piezo can be controlled in open-loop or closed-loop mode. The servo-loop logic compares the control voltage input and the position sensor signal to generate the power amplifier input control signal. An analog proportional-integral (P-I) algorithm is used. Whit the servo-loop algorithm, the drift, nonlinearities and hysteresis effect of the PZT actuator are compensated. In the figure 4.9 the Servo-loop block diagram is shown.

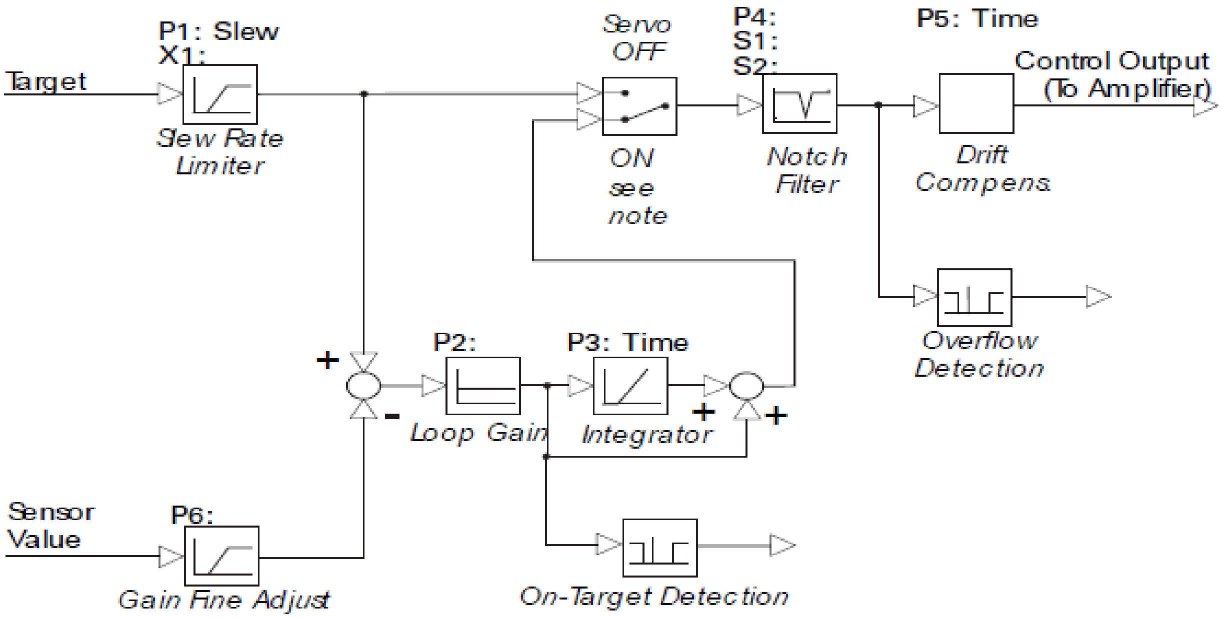

Figure 4.9: Servo-loop block diagram.

Slew rate limitation insures that the output signal slope does not exceed the following capability of the power amplifier. The notch filter is used to damp out oscillation at the resonant frequency of the mechanics. Position information is provided by high-resolution sensors integrated in the mechanical stage or PZT actuator. The effective stiffness of the actuator is significantly increased due to the rapid displacement control effected by adjusting the PZT operating voltage so as to maintain the displacement even when external forces change. The sensor monitor socket allows to monitor the analog output using an oscilloscope. The 'T' and 'P' socket are respectively target signal and probe signal of PZT. With the switch 'Servo' in ON, the closed loop mode is activated.

- **Digital Interface**

The E-518.I3 is a microprocessor controlled interface for the E-500 piezo controller system. This module allows to control PZT with digital interface. The digital control signal is converted to analog and sent to the Sevo-Controller module. The E-518 supports several programming languages as C, *C++, Python, Matlab, LabView.* It can be connected to host PC via USB or LAN connection. The software used to interface with the device is

PIMikroMove™. This software provided by the PI company is a graphical user interface for Windows. Thanks to this software can be controlled the PZT either in open-loop or closed-loop operation and getting graphical results of its response to the command. The two most important features of this module are the *Wave Generator* and *Data Recorder*. The integrated wave generator can output periodic motion profiles. This feature is especially important in dynamic applications which require periodic, synchronous motion of the axes; in particular it was used to generate a sinusoidal command. The data recorder allows to record the output signals (e.g. current position, control voltage) with a maximum rate of $40\,\mu s$ per point. This data can be exported in *.csv* or *.dat* format and used in the Matlab scripts for the post-processing. More details are specified in the section 5.1.

The interconnections between the three modules is shown in the diagram in the figure 4.10. The digital signal, created by software, is converted to analogue (TARGET OUT) and sent in the E-509 module. The 'TARGET IN' is processed by the servo loop logic. When the Servo toggle switch is ON, the closed-loop logic is activated. The target signal is compared with the sensors signal and the control output is generated. The 'SERVO-CONTROL OUT' is voltage required to reach the commanded position. It is the input of the power amplifier. The voltage is amplified with a specific gain and will supply the piezo actuator. In analog operation, the digital module is bypassed. The 'SENSOR OUT' can be monitored via *Data Recorder*. The signal is recorded on the integrated memory card and converted from analog to digital. It is possible to monitor the analog signal output with an oscilloscope.

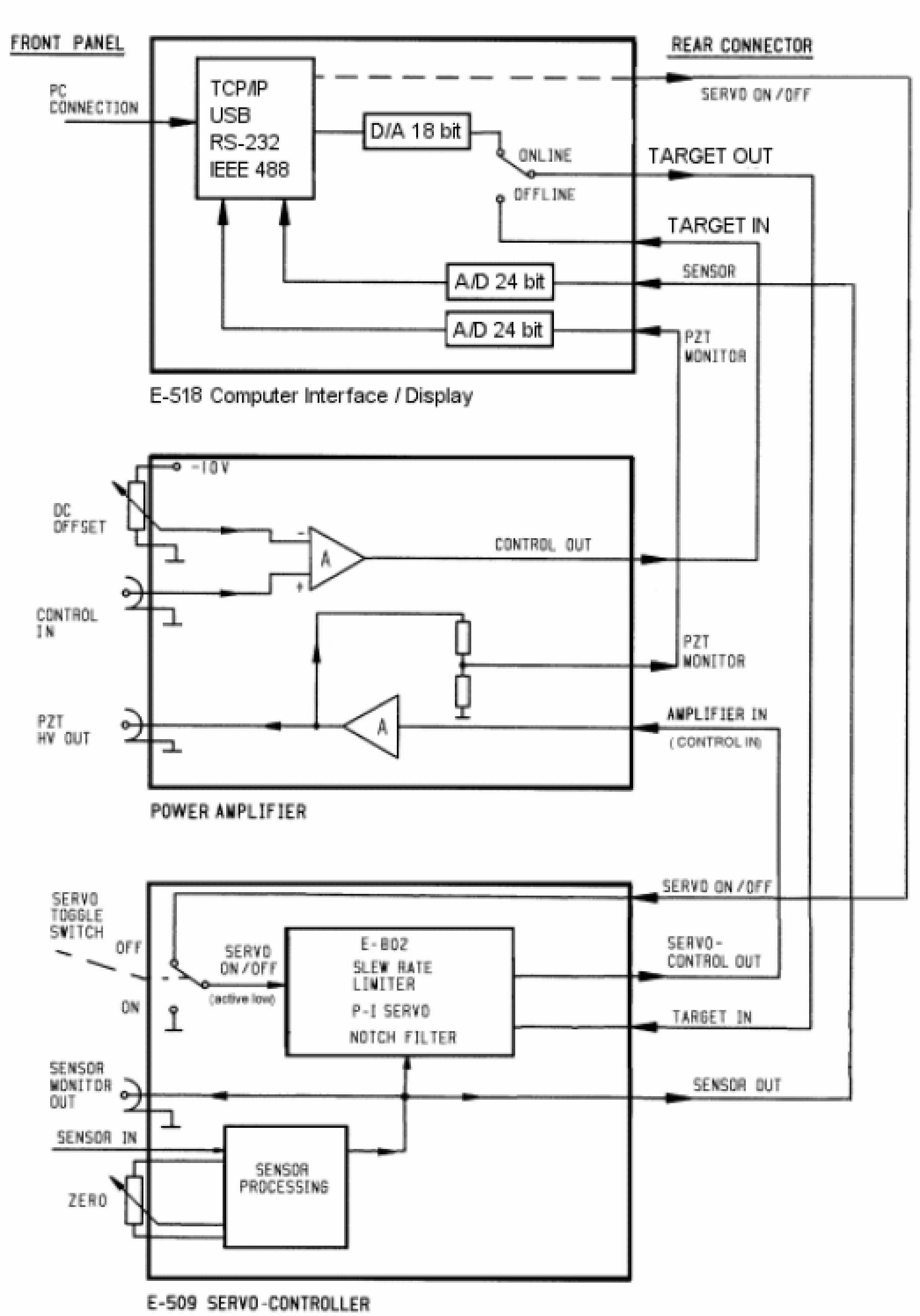

Figure 4.10: Interconnections between E-518 digital piezo controller operation module, amplifier module and E-509 servo module

4.3.2 Frequency Generator

During the preliminary tests, a frequency generator was used to control the PZT in analog mode. It was connected to the amplifier module via the Control Input socket. A sinusoidal signal has been generated with amplitude between 0 and $10V$, with an offset greater than zero. Voltage amplitude is converted into a positional amplitude by servo-loop logic. The digital module, in analog operation, has been used to save the output signal via *Data Recorder*.

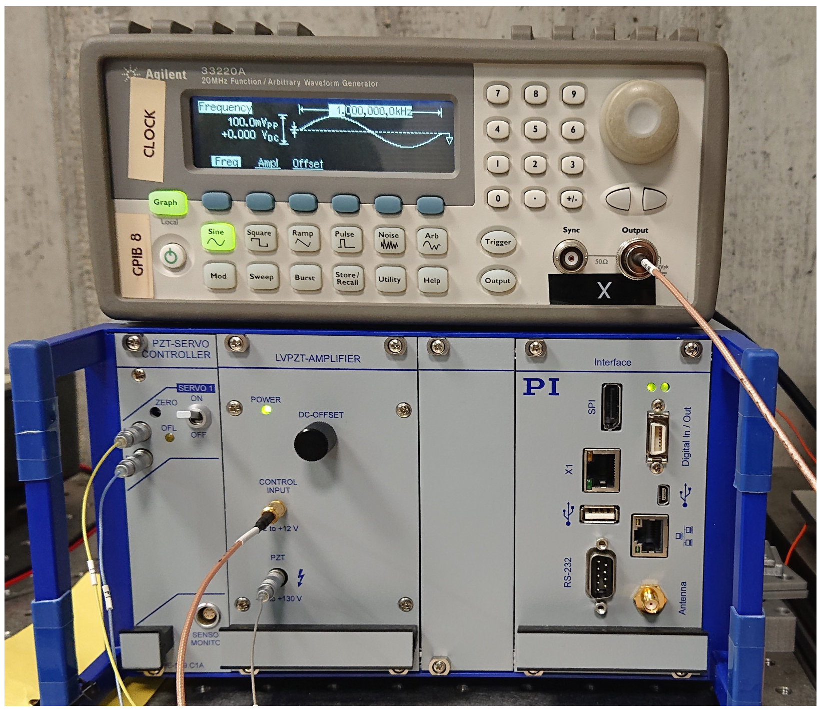

Figure 4.11: Function/Arbitrary Waveform Generator connected to E-500 device

4.4 CAD design

In this section, the parts made by CAD design are illustrated. *Solidworks* has been used as CAD software. Some components are made of PLA or aluminium, depending on their use. The parts were used for the assembly of the devices on the test bench and for the optical fiber locking system. The components are detailed below.

4.4.1 Aluminium plate for Piezo device

P753.31C device was mounted on the breadboard using an aluminum plate. P753 must be mounted on a flat surface and with a recommended surface uniformity $\leq 10\,\mu m$. In order not to add extra compliance to the system, it was preferable to use aluminum because the P753 is made of the same material.

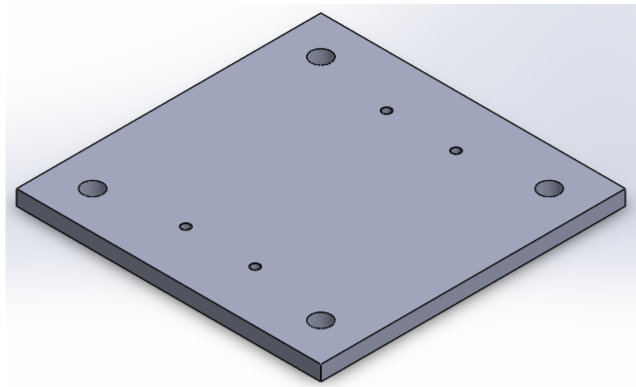

Figure 4.12: Aluminium plate for Piezo device

The aluminium plate has a size $100 \times 100 \times 5\,mm$. It has 4 holes for mounting on the breadboard with M6 socket head cap screw and 4 threaded holes for mounting the piezo with M3 pan head cross recess screw.

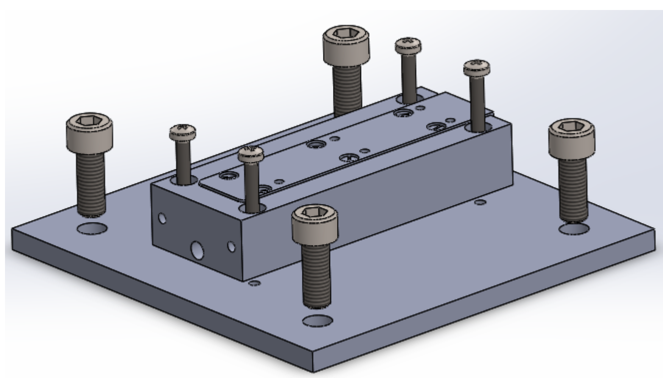

Figure 4.13: Piezo P753 and plate assembly

4.4.2 Aluminium plates for Micropositioner

The micropositioner has been used for fibre tensions. In fact, as will be shown later, the fiber has been fixed on the micropositioner and on the piezo. The micropositioner allows displacements along the x-axis in the order of hundredths of a millimeter. An aluminum plate has been designed for mounting on the breadboard.

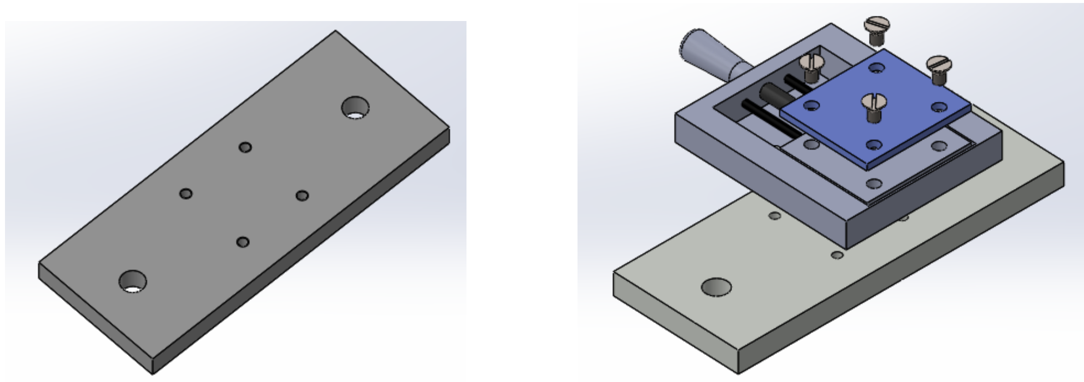

Figure 4.14: Aluminium plates for Micropositioner and micropositioner cad assembly

The aluminium plate has a size $100 \times 40 \times 6,7\,mm$. The dimensions of this plate have been designed to perfectly align the piezo and the micropositioner. In the plate there are two holes for fixing on the breadboard and four holes for M3 screw to fix the micropositioner.

4.5 Locking Systems

Several optical fiber locking systems have been the subject of previous studies in other thesis. The best solution chosen is based on the locking system with epoxy resin. For tests of frequency response of the FBG sensors, the fiber was fixed at two points with the Bragg gratings approximately in the middle. Specifically, it is fixed on the micropositioner and on the piezo. Rectangular plates were used to fix the fiber on both devices. As shown in the figure 4.15, the plate is mounted on the micro-translation stage and then the fiber is glued to the plate.

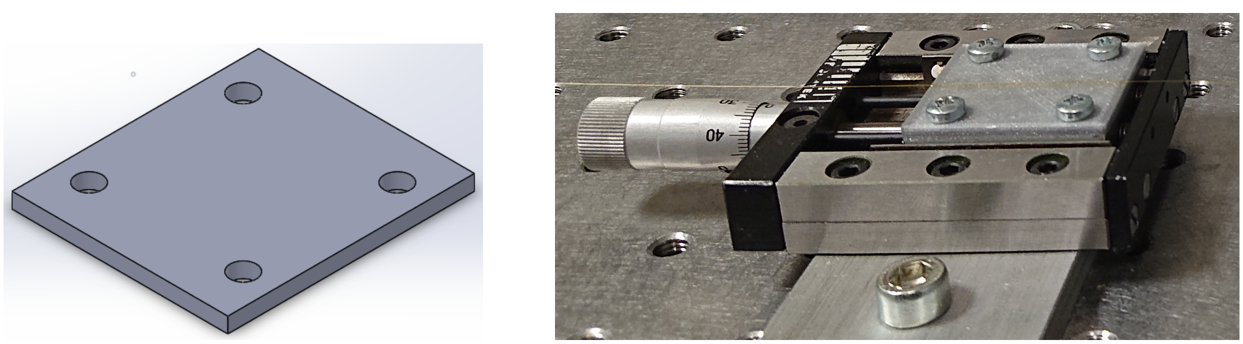

Figure 4.15: Plate for micro-translation stage

On the other side, a plate has been designed to be mounted on the PZT stage. This rectangular plates has the same size of the moving surface of the piezo. The thickness of the plates is $2\,mm$.

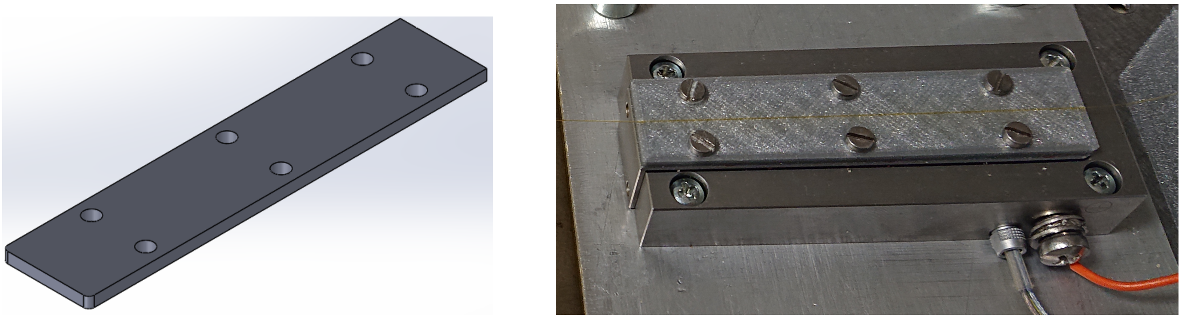

Figure 4.16: Plate for PZT actuator

These plates were made in PLA by 3D printing. It is possible to remove mechanically the resin glued on the plates, but this operation could cause the damage of the components. For this reason, a new plate is required for another gluing. The two stages with glued fibre are shown in the figure 4.17.

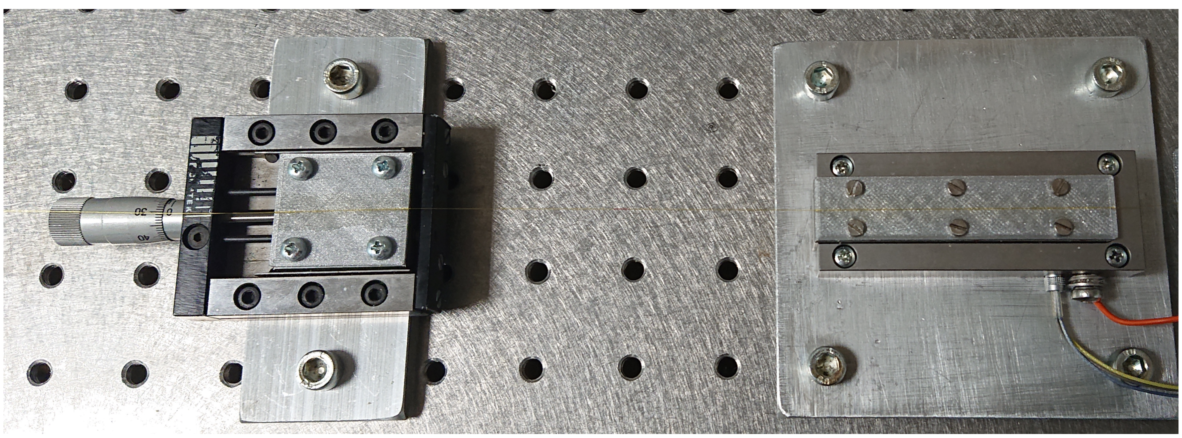

Figure 4.17: Locking system in detail

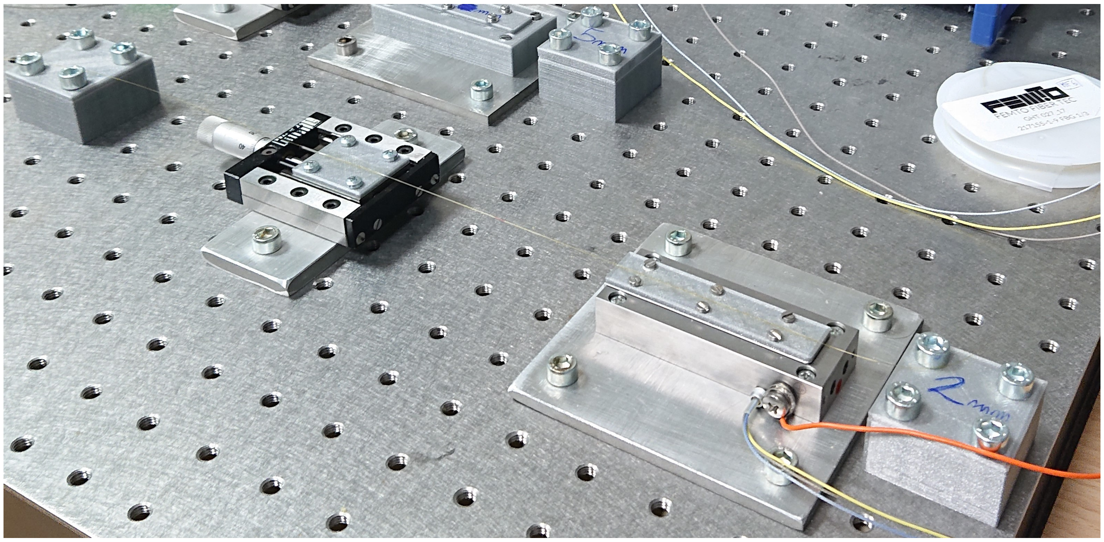

Figure 4.18: Complete locking system assembly

The plates are fixed on the stages and afterwards the optical fiber is glued in a central position. The fiber is thus perfectly aligned. The fiber is glued with an initial manual pre-tensioning. To hold this tension during the drying phase (approx. 18 hours), the fiber is fixed to a blocks in PLA (places behind the two stages) with adhesive tape (fig. 4.18). The initial length L_0 is defined as the distance between the end of gluing points. Different measurements and results are obtained by varying the initial length L_0. It is possible to apply a load in terms of strain ($\mu\varepsilon$) variations or ΔL on the fiber by using the micropositioner.

Another gluing station has been installed on the test bench. This is a copy of the main station. The same micropositioner is used for tensioning the fiber optic during gluing. Instead, a copy of the piezo was designed and made in PLA (fig. 4.19)

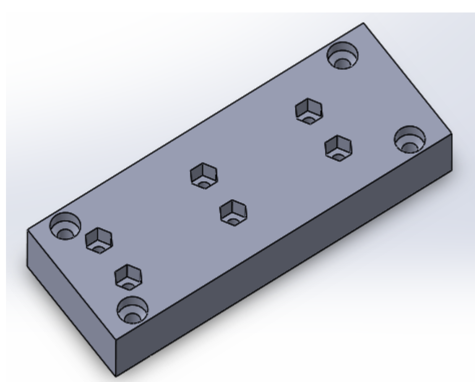

Figure 4.19: Part similar to piezo actuator

As shown in the figure 4.19, the component has the same dimensions as the PZT stage. There are hexagonal inserts in the upper surface. These allow hexagonal nuts to be inserted for mounting the gluing plate.

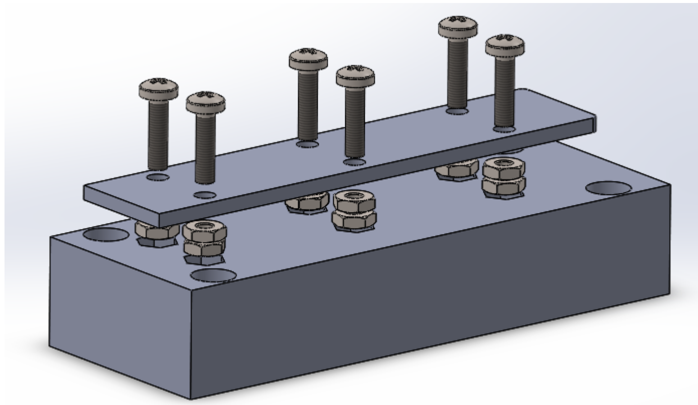

Figure 4.20: View of the assembly for mounting the plate

The plates used for mounting the components on the breadboard are the same as those described in the section 4.4.

At this station the fibre is glued and then used for tests in the main station. When the glue is dry, it is possible to unscrew the plates from the microfeeder and the similar piezo. With great caution, they are moved and mounted on the main station. After assembly of the plates, the fibre is tensioned with a micropositioner. The complete assembly of the secondary station is shown in the figure 4.21.

Figure 4.21: Complete assembly of the gluing station

The distance between the components mounted on the breadboard is determined by the length L_0. This length has a significant influence on measurements. In fact, L_0 corresponds to a Bragg wavelength (λ_{B_0}). From this value the tests are performed and the microstrains of the fiber are calculated as:

$$\mu\varepsilon_{fiber} = \frac{\Delta\lambda_B}{\lambda_{B_0}} \tag{4.2}$$

where the variation of the Bragg wavelength $\Delta\lambda_B$ is calculated as a variation of the length ΔL. The L_0 is also used for calculating the microstrains of the piezo as:

$$\mu\varepsilon_{PZT} = \frac{\Delta L_{PZT}}{L_0} \tag{4.3}$$

where ΔL_{PZT} is the real position of the piezo reached during dynamic motion. In chapter 5 the use of these relations is explained in detail.

Chapter 5

Softwares for the tests

This chapter shows all the software and matlab programs used during the tests. The two main softwares are PIMikroMove and SmartSoft. The first is the graphical interface of the modular piezo controller. It allow to send displacement command to the PZT actuator. In particular, a tool of this software is used to create a sinusoidal command: *PI Wave Generator Tool*. The second software is the graphical interface of the SmartScan interrogator. Using this software, it is possible to record the data received from the FBG sensor connected to the interrogator. After a test the data of both software are saved. For the post-processing of these data files are used matlab programs implemented for the purposes of this thesis. Each software is described in the following sections.

5.1 PIMikroMove

Modular piezo controller described in the paragraph 4.3.1, it is controlled in digital mode with the software interface *PIMikroMove*. It is a graphical user interface for PZT stage motion controllers. It is installed on the host PC using the CD provided by the PI company. *PIMikroMove* allows you to immediately start the motion system without the need to write customized software. The program relies on the GCS DLL for the controller communication. Connection to the digital module (*E-518)* is via USB or LAN. After connecting the host PC, launch the software and establish the connection with the controller E518. The use of the software is detailed below.

The main window shows the stage connected to the Servo Module. Only one PZT stage is connected to the E-509 module. So only the *A:A* axes is active (fig. 5.1). The software allows to control the PZT in open-loop and in closed-loop. To switch from one servo-mode to another, check the Servo box. Alternatively, to activate closed loop servo-mode, switch the 'Servo' (in the *E-509* module) to 'ON'. For our purposes, the PZT has only been controlled in closed-loop mode.

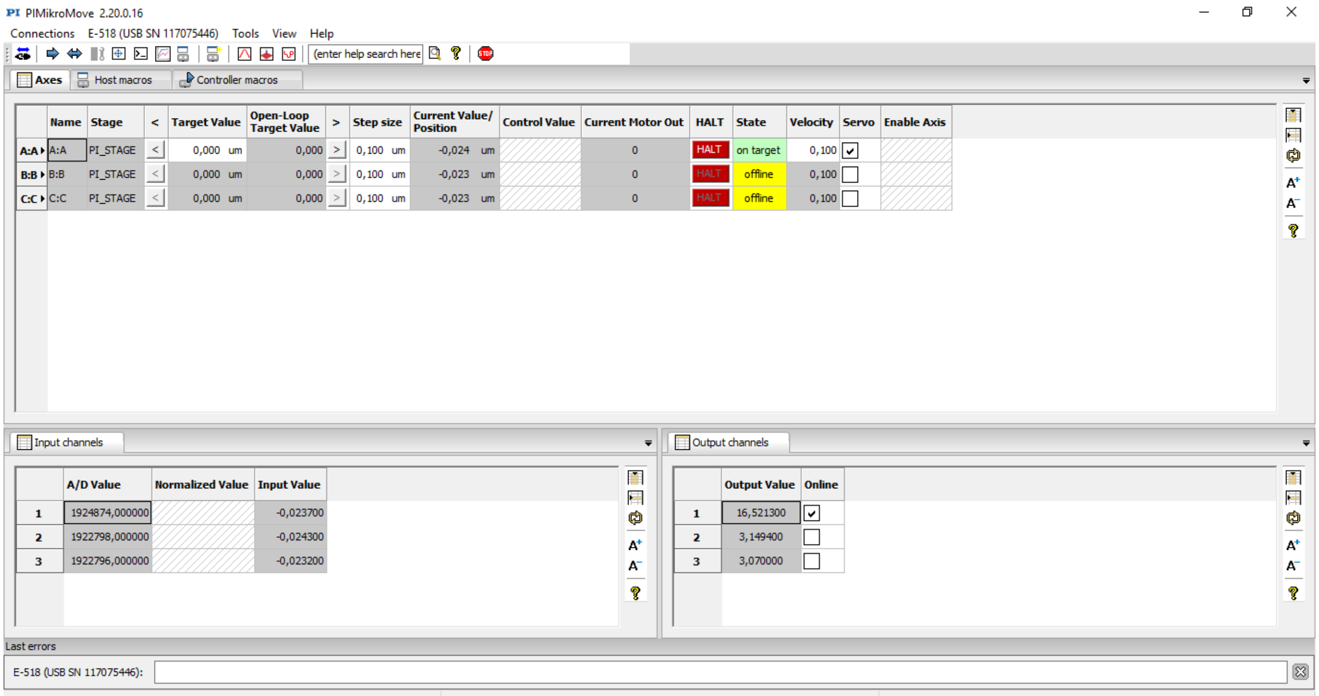

Figure 5.1: *PIMikroMove:* the main window.

All the procedures explained below are in closed-loop mode. The '*Target Value*' box is the piezo-controlled displacement value. By writing a value between $0 - 38\,\mu m$ (maximum travel), the piezo will be controlled in voltage obtaining the desired position.

The PZT was used to induce dynamic strains in the optical fibre. For this application, we used the *PI Wave Generator Tool*. This is a *PIMikroMove* tool that allows to generate a waveform signal.

5.1.1 PI Wave Generator tool

This tool has always been used with the 'Servo' switched on (closed-loop mode). Thus, the PZT was controlled in displacement by a waveform signal. *PI Wave Generator* was used to create a sine waveform, as shown in figure 5.2.

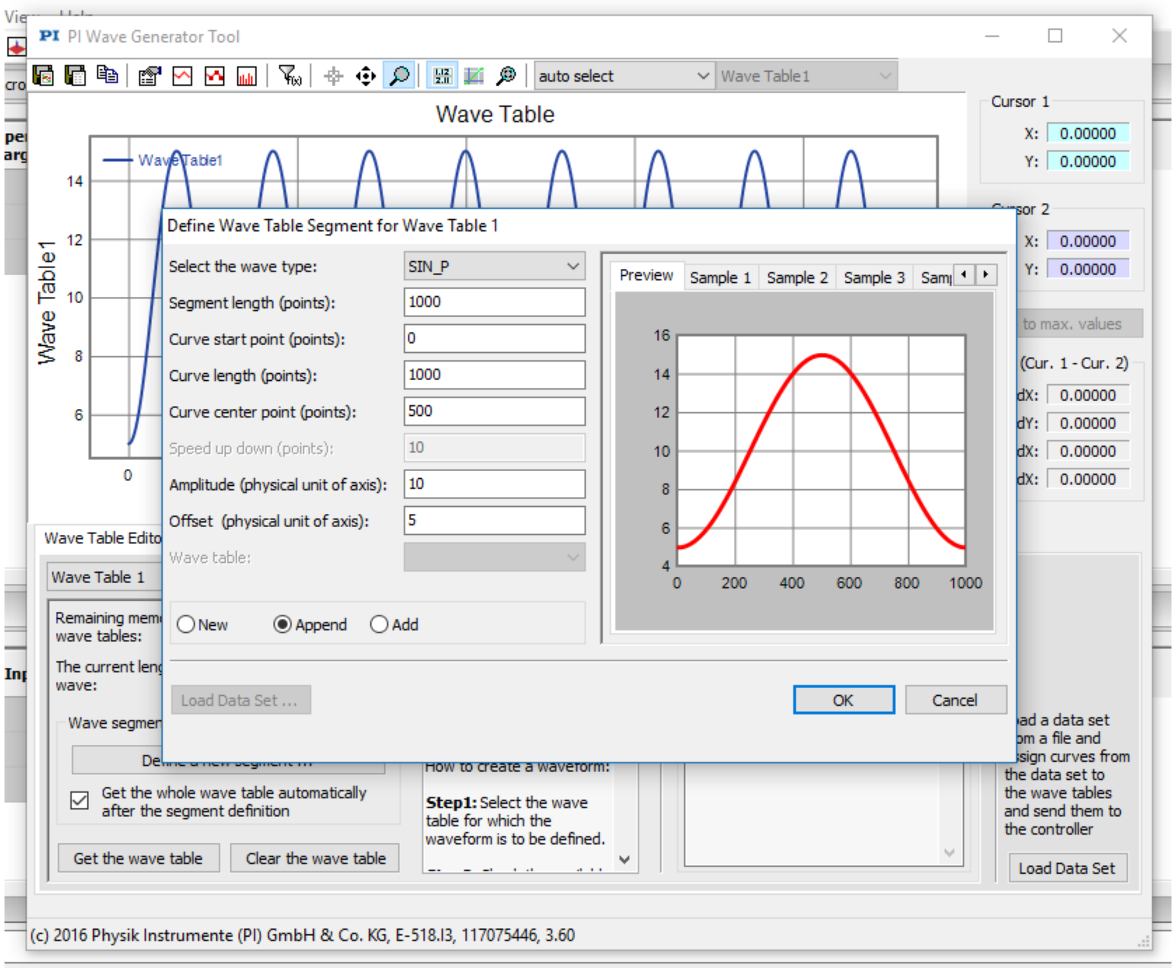

Figure 5.2: PI Wave Generator Tool: define wave table segment

The E-518 module cannot generate waveforms with arbitrary frequencies. It can change the output voltage only once every 40 μs. Therefore, the period of the waveform must be a multiple of 40 μs. The waveform is created for points with a maximum of 8192 points per wave table. The sinusoidal period and frequency are calculated according to the relations:

$$T = Points \times 40 \cdot 10^{-6}\, s \tag{5.1}$$

$$f = \frac{1}{T} \tag{5.2}$$

The minimum frequency that can be created is $3.052\,Hz$. To increase the frequency, it is necessary to create a wave with fewer points. Under 20 points the wave is not exactly defined. This limit is not a problem because the maximum operating frequency of the piezo is of $1\,KHz$. The maximum frequency used in the tests was $300\,Hz$.

The waveform is created in *Define Wave Table Segment for Wave Table* window. The number of points of the *Segment Length* defines the period of oscillation of the wave according to the equation 5.1. *Curve length* is the number of points that interpolate the sinusoid. By changing the values of *curve start point* and *curve center point*, we obtain the sinusoidal curve shown in the figure

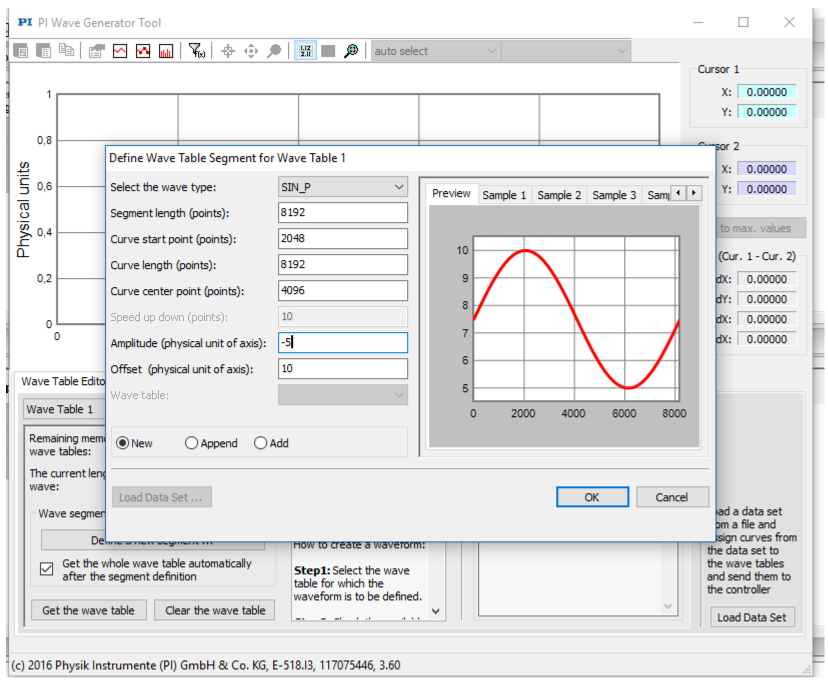

Figure 5.3: Define wave table segment

In closed-loop, the values of *Amplitude* and *Offset* are relative to displacements in μm. By clicking on *New* the first wave is created. If you want to add more consecutive waves, click on *Append*. The maximum number of waves that can be stored is given by the whole part of the ratio between the maximum number of points (8192) and the wave length. Figure 5.4 shows an example of a waveform created.

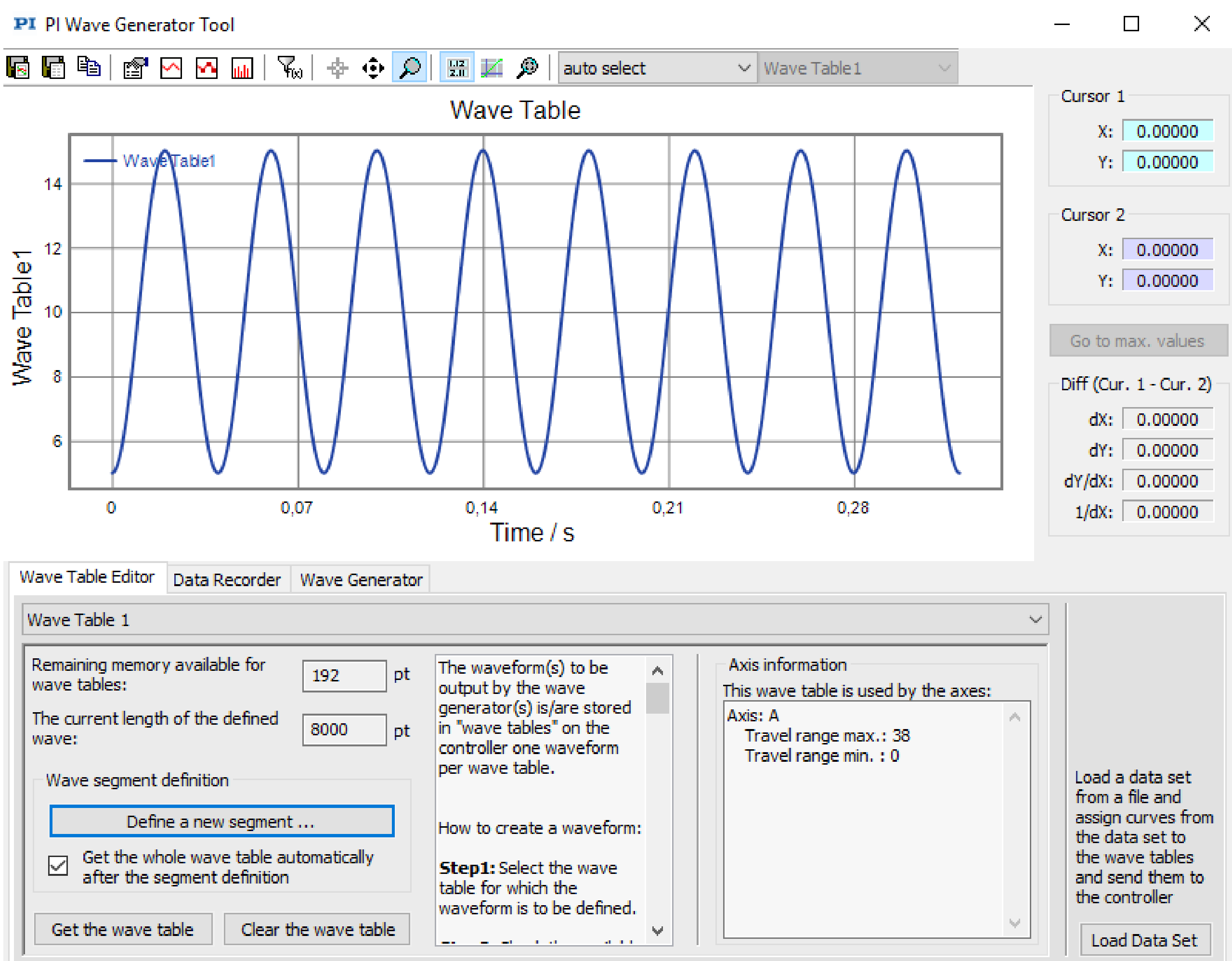

Figure 5.4: PI Wave Generator tool: Wave Table Editor

8192 points are also the maximum number of points that can be recorded by the *data recorder*; it is thus possible to record a maximum period of $0.32\,s$. In the *Data Recorder* section you can output a longer recording period by increasing th*e Record Table Rate* parameter. To avoid aliasing problems (at high frequency), this parameter has been set to 1 (i.e. sampling takes place every $40\,\mu s$).

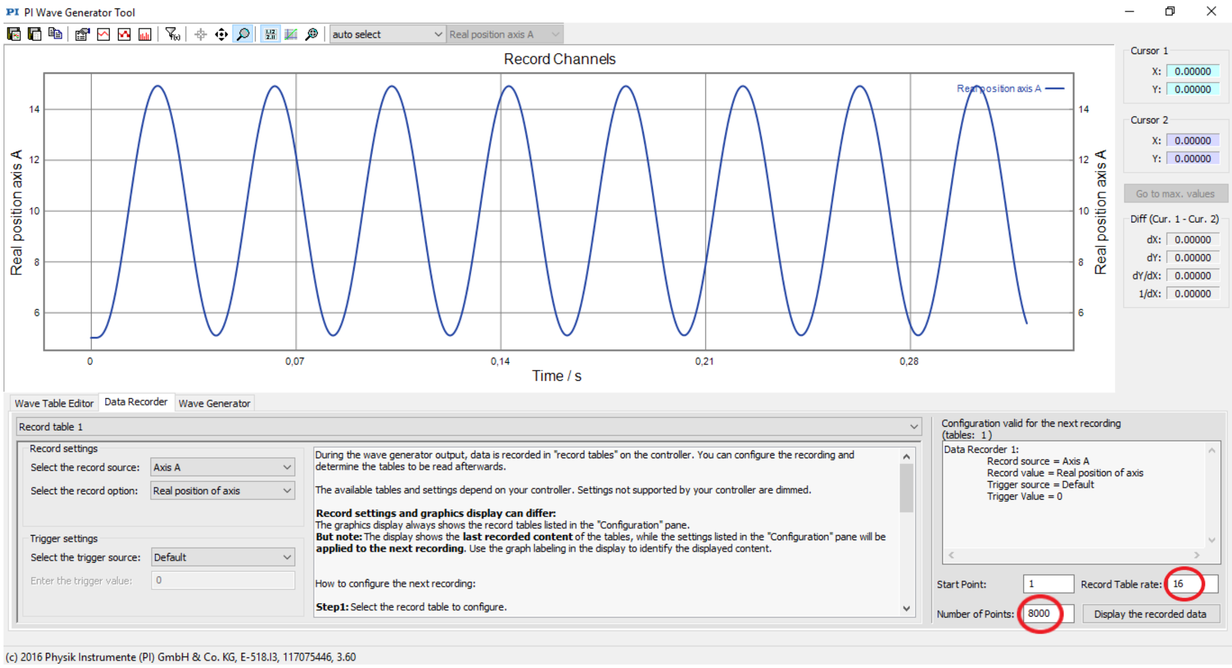

Figure 5.5: PI Wave Generator tool: Data Recorder

The duration of piezo activation is set in the wave generator window. The number of cycles determines the time of the duration of the command. A cycle is the total period of the succession of semi-waves created in wave table editor. Clicking on *Run Wave Generator* the command is sent to the controller that will drive the PZT. If the value of the number of cycles is set to 0, the dynamic of the PZT ends only when you click on *Stop Wave Generator*. When the wave generator stops, clicking on *Display the recorded data* the graphic of the piezo response is shown (fig. 5.6). The outputs to be shown in the graph are configurable. Of interest to us were the voltage and the real position. The voltage has been monitored to verify that it is within operating limits. The real position was exported by saving the data in the *.csv* format and used in post-processing.

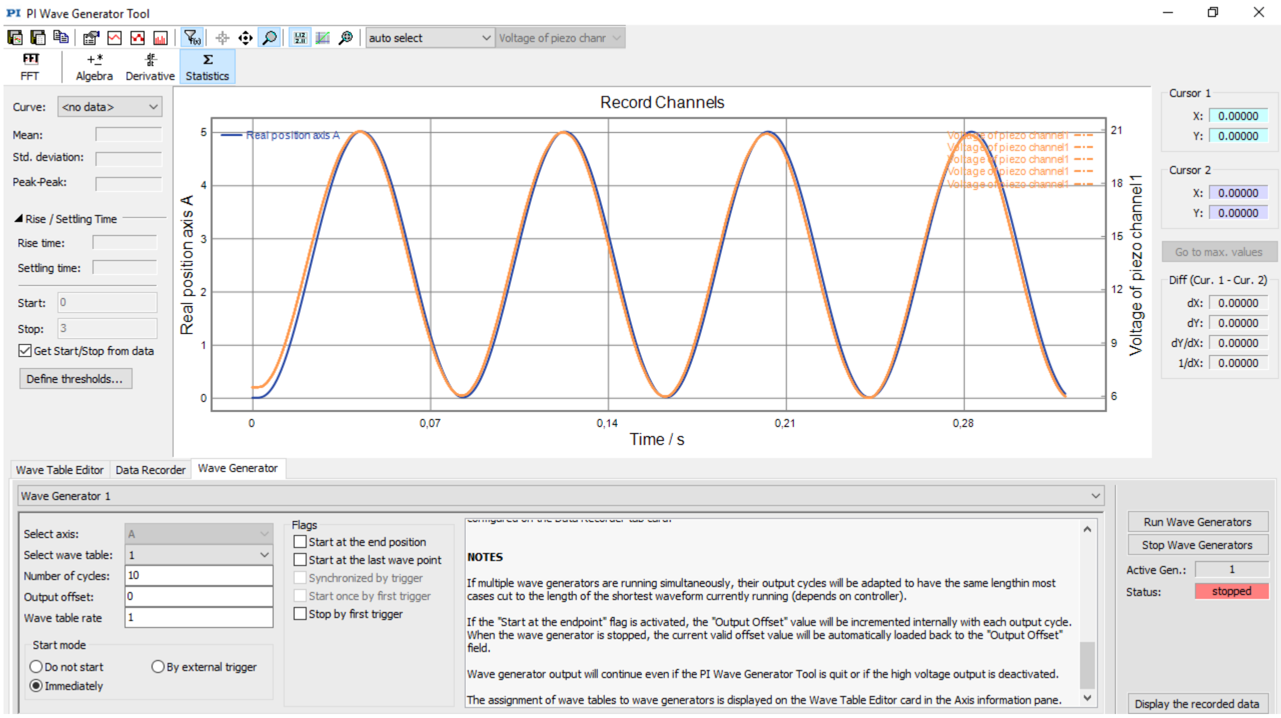

Figure 5.6: PI Wave Generator tool: Wave Generator window

5.2 SmartSoft

The *SmartSoftSSI* software is the graphical interface of the SmartScan interrogator. It allows you to monitor and record the signal sent from the interrogator. When the program is started, the connection via ethernet is established. The main window is shown in the figure 5.7

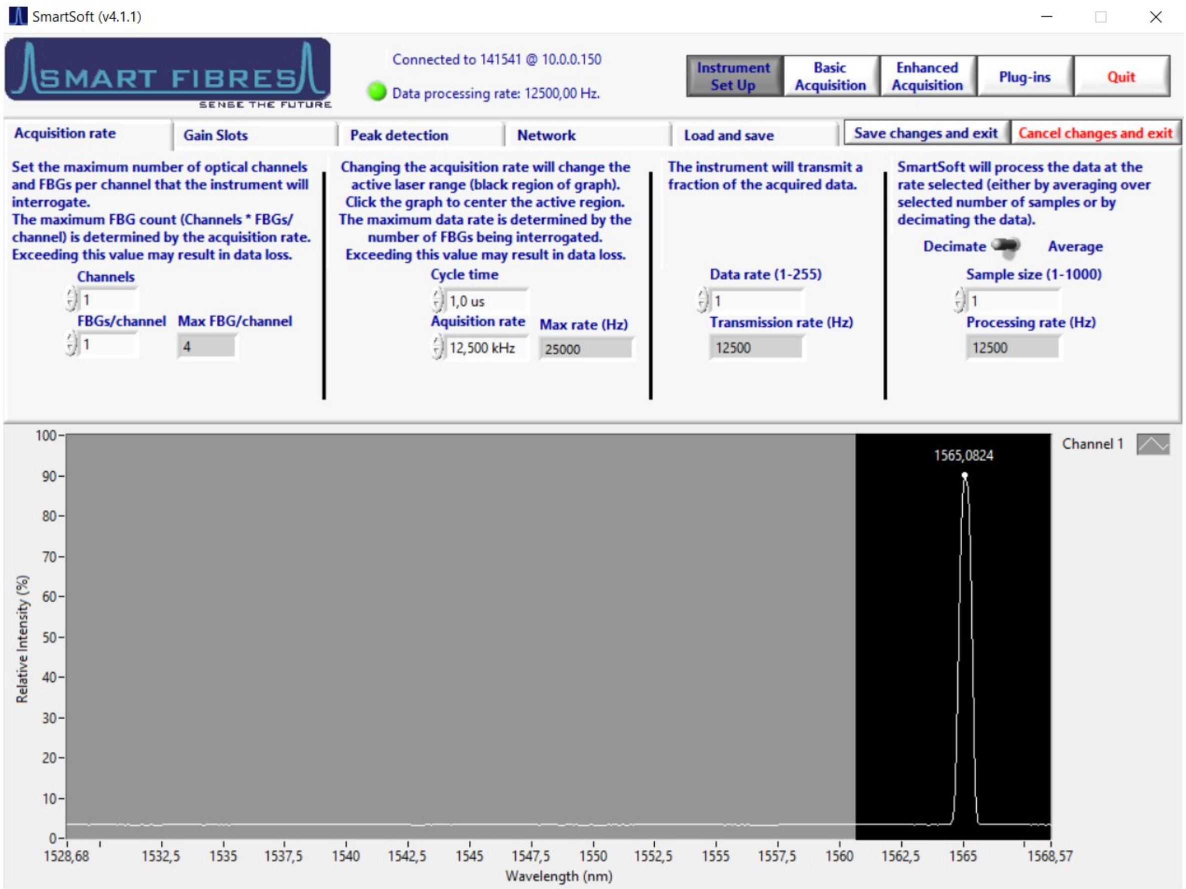

Figure 5.7: *SmartSoftSSI:* main window

The graph (spectrum tab) displays the Bragg wavelength (reflected signal intensity) with the maximum peak value. Each peak is relative to the respective FBG sensor. In the first section, it is possible to set the number of channels used and the number of Bragg sensors. Each channel is connected to a fiber that can have more than one Bragg sensor. In the *Acquisition Rate* box, it is possible select the sampling rate; in our tests is set to 12500 Hz (i.e 80 μs). This frequency allows a suitable sampling without aliasing problems. By increasing the acquisition rate, the active laser range will be reduced. The inactive range will be greyed out in the graph. The SmartScan cycle time in microseconds (μs) can be adjusted. The cycle time is defined as the time to complete one laser tuning step and measure the light received by the detector circuits. This can speed up or slow down the overall acquisition time. The minimum cycle time is 1 μs. The data rate is set to 1. This means that the SmartScan will transmit all available data to the PC and the transmission rate will be equal to the acquisition rate. The number of data to be saved in the log file is set in the sample size box. If it is set to 1, any transmitted data will be saved.

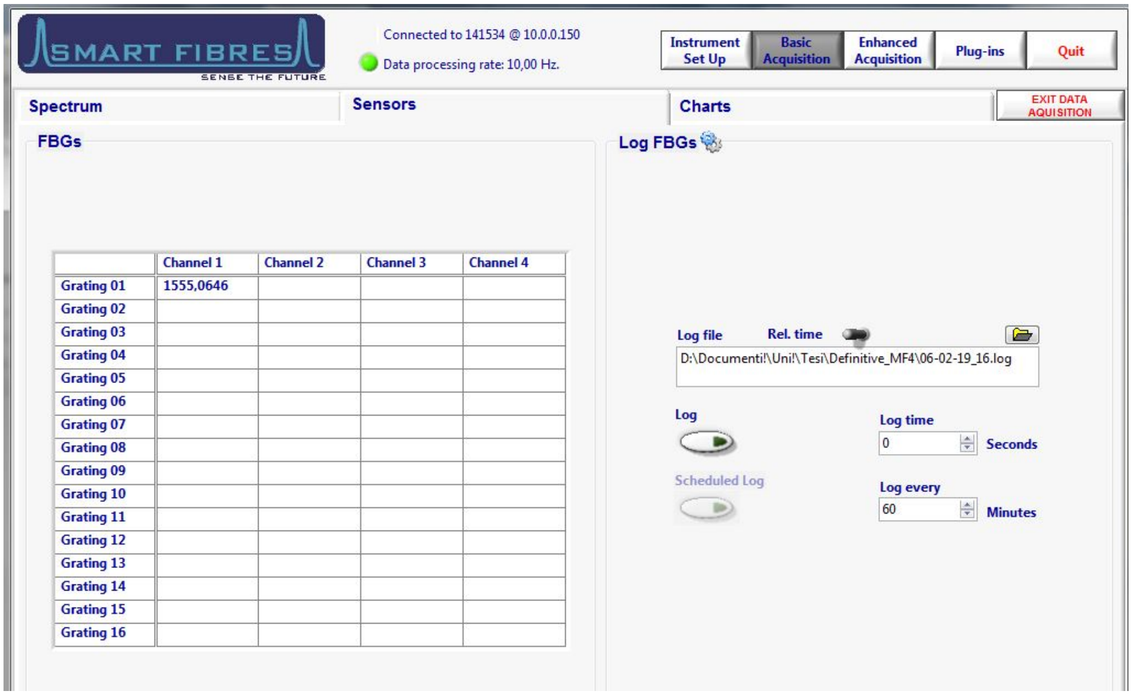

Figure 5.8: *SmartSoftSSI:* Basic Acquisition section

After setting these parameters you can proceed with the data acquisition. In the Basic Acquisition section, it is necessary to set the folder address and the file name with the .log extension. Then set the acquisition time in Log time box and click on Log to start. The saved file can be used by matlab programs for data analysis.

5.3 Matlab programs

This section describes the *Matlab* programs developed specifically to facilitate the creation of the wave in the *PI Wave Generator Tool* and for data post-processing. All *Matlab* scripts are stored in the *Program_Matlab_PZT* folder. Inside there is a sub-folder called *Script*. The programs stored in this sub-folder are detailed below.

- ***Calcolo_frequenza_punti:*** It is used to create the wave. It provides all the data to be entered in the *PI Wave Generator Tool*. The user provides in input the frequency of the sinusoidal wave to be obtained, the number of half-waves and the duration of the test. Equations 5.1 and 5.2 have been used for these calculations In output you will have the number of points and the number of cycles.

- ***Post_processing_3_1:*** This program is developed and used in previous thesis. It allows to open and read the file exported by the *SmartScan* interrogator software. The data are processed and returns in output the vector time (duration of the test), the vector wavelength (λ_B) and the vector of the mechanical strain. The mechanical strain are calculated using the equation 3.9, where the gauge factor K_ε is set to 0.78. An example of graphic results are shown in the figure below:

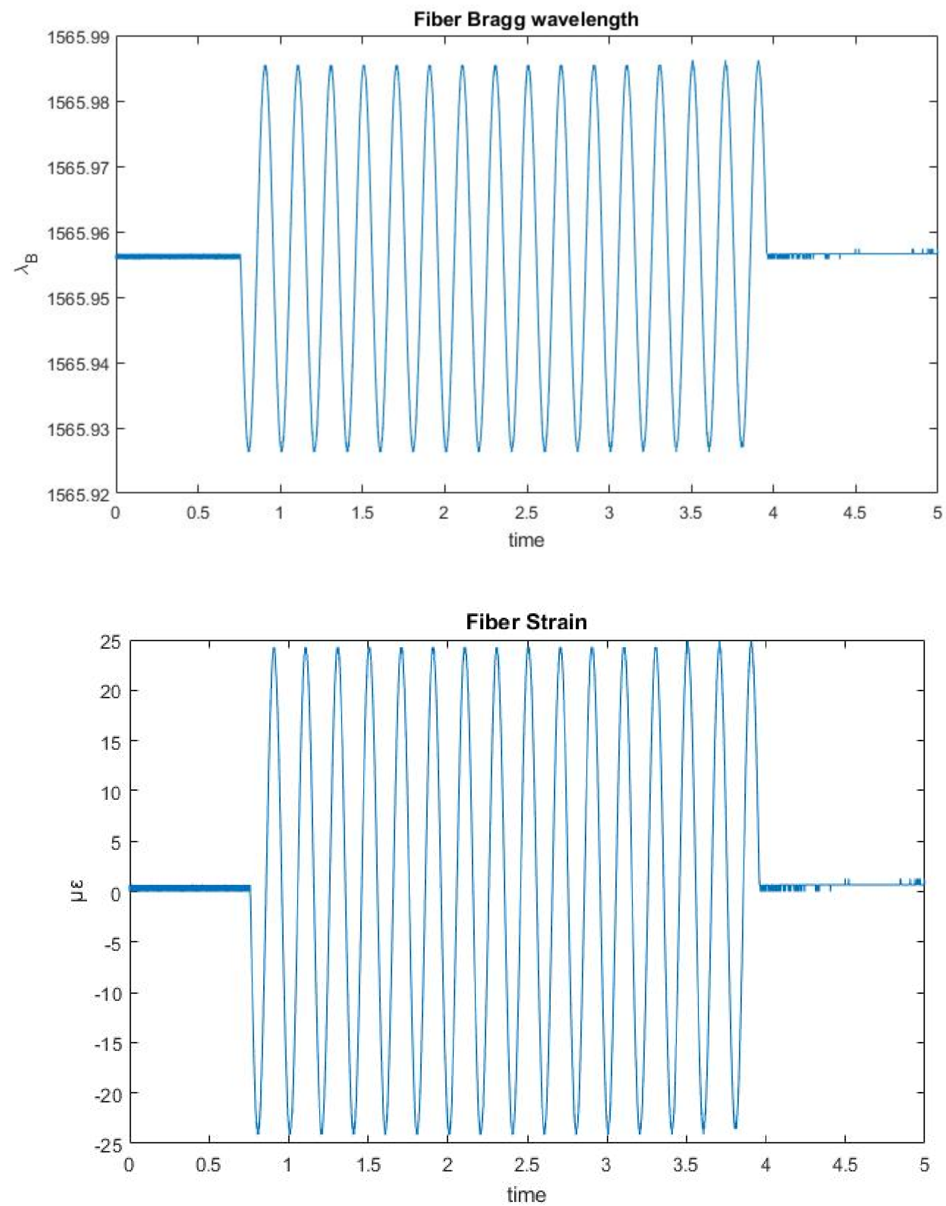

Figure 5.9: Graphs of the recorded wavelength (λ_B) and calculated microstrains ($\mu\varepsilon$)

- ***Apertura_file_csv_piezo:*** The file exported from the *PIMikroMove* software must be in *.csv* format and placed inside the script folder. The user enters the file name. The program reads the file and saves the data in a matrix.

These three main applications have been implemented in a single matlab script: ***Analisi_Dinamica***. This program allows a complete analysis of the tests carried out. It is divided into three parts: pre-processing, processing and post-processing. In the pre-processing, the characteristics of the waves are acquired. In this part is run the script *Calcolo_frequenza_punti.m*. The user enters the wave characteristics for the sinusoidal command. These parameters are then entered into the *PI Wave Generator Tool*. After testing the fiber, the two files of the PIMikroMove and SmartSoft software are exported and stored in the "script" folder. Now, it is possible to continue in *Analisi_Dinamica* with the processing of the data. The user enters the name (with the extension *.log*) of the file exported by the SmartSoft software. In this part is run the script *Post_processing_3_1*. After executing the required commands the data will be loaded and stored in structures. Next, *Apertura_file_csv_piezo* is run. The user enters the name (with the extension *.csv*) of the file exported by the PIMikroMove software. Data recording from PiMikroMove and SmartSoft software takes place at different times. In the post-processing part, the program implements a synchronization of the data vectors of the fiber and the piezo. To establish the start of the test, the first variation of the fibre microstrains must be detected as an initial instant. A tolerance of about 1.9 $\mu\varepsilon$ is used to avoid the risk of taking a value of fluctuations in the signal. This tolerance When the initial time of the test is established, the data carriers of the fiber are cut off. In this way, vectors are obtained with the effective measurement The interrogator acquires data every $80\,\mu s$ while the piezo every $40\,\mu s$. The time and position vectors of the command are modified by removing one cell every two so as to have a step of $80\,\mu s$. The piezo controller records only the first cycle performed. The program performs the search of the maximum and minimum peaks of the fiber microstrains. These are calculated from the second-last cycle when the fiber is in full operation. The search for maximums and minimums of the piezo microstrains (4.3) takes place on waves that are after 75% of the total number except the last one. Then, the mean values of the maximums and minimums respectively are calculated. Now, it is calculated the amplitude of the piezo and fiber microstrain. The amplitudes are calculated with the following relationships:

$$Amp_{fiber} = |max_{fiber} - min_{fiber}| \tag{5.3}$$

$$Amp_{PZT} = |max_{PZT} - min_{PZT}| \tag{5.4}$$

$$dB_{amplitude} = 20\log\frac{Amp_{fiber}}{Amp_{PZT}} \tag{5.5}$$

The bode amplitudes (5.5) at different frequencies are reported on an Excel file. This file is used in the *Diagrammi_bode_sperimentali* program. This matlab script allows to plot the experimental bode diagram. The program reads and saves the data of the Excel file.

Insert test specification: amplitude of the command, effective length of the fiber.				BODE FIBER				
FREQUENCY (Hz)	COMMANDED AMPLITUDE (μm)	REAL AMPLITUDE (μm)	THEORETICAL AMPLITUDE (μm)	TEST 1	TEST 2	TEST 3	TEST 4	AVERAGE VALUE [dB]
5								
10								
20								
25								
50								
75								
100								
150								
200								
250								
300								

Figure 5.10: Excel file template

Data is interpolated with the method of the least squares. Then for several tests, the diagrams are plotted and saved.

For more details on matlab programs see the thesis of Gioele Baima [1].

Chapter 6

Test and measurements

Several tests have been conducted to investigate the dynamic response of the FBG sensor. A linear piezoelectric actuator was used to induce dynamic strains in the optical fiber. The actuator is controlled by a sinusoidal command at several frequencies. The Bragg grating is thus subjected to vibrational stresses. The variations of wavelength reflected by the grating are recorded by the FBG interrogator. Using the softwares described in chapter 5, it is possible to perform the tests and process the data using the matlab programs that were created for this purpose. The optical fiber tests have been performed with the layout shown in chapter 4 (fig. 6.1). This chapter describes in detail the tests carried out and the measurements resulting from them.

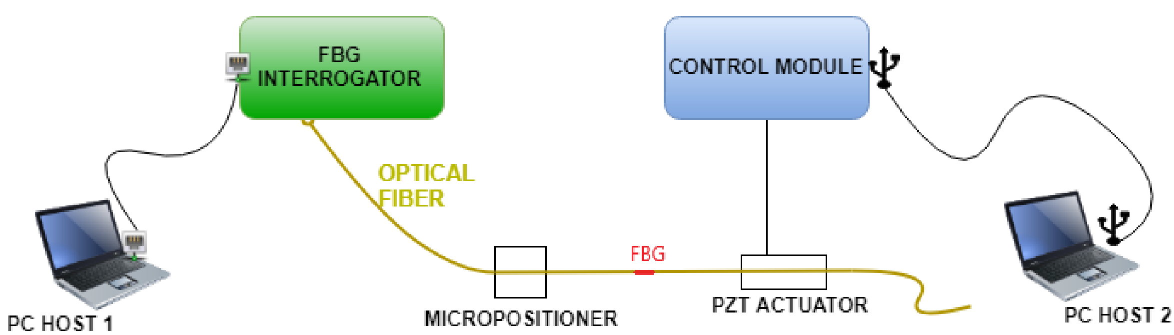

Figure 6.1: The chart of hardware.

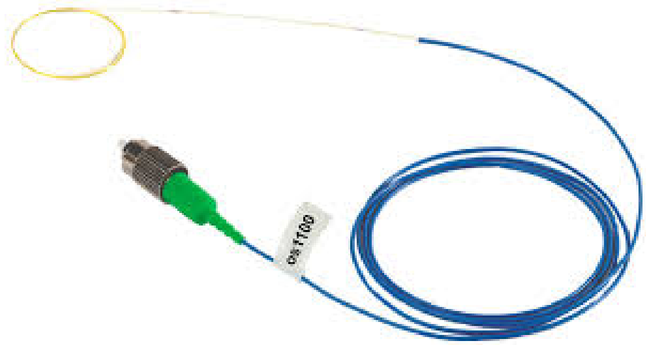

Figure 6.2: The optical fiber used.

The optical fiber used for the tests was manufactured by FEMTO FIBER TEC. The fiber has a core diameter of 9.8 μm , a cladding diameter of 125 μm and a polyimide coating with diameter of 155 μm. Polyamide coating protects the fiber, especially against water and hydrogen which causes crack growing and can reduce the mechanical stability. In the fiber there is only one FBG inscribed. It has a length of 3.2 mm with a center wavelength of 1565.07 nm. To be able to use it has been connected to an optical connector, also for a segment has been protected by a outer jacket (fig. 6.2).

6.1 The tests

First dynamic analysis tests were carried out at low frequency. A command amplitude was chosen and three consecutive tests were conducted at each frequency. The bode diagrams were plotted for each test. In addition, a bode diagram was plotted using the average value. It is important to remember that the free length of the optical fiber is $L_0 = 0.1\,m$ (i.e gluing distance). This length is important for the calculation of microstrains (4.2, 4.3). The frequencies used are shown in the table.

3.0517 Hz	5 Hz	10 Hz	20.49 Hz	30.49 Hz	50 Hz

Table 6.1: Low Frequencies used in the tests

It is possible to note that some chosen frequencies are not integer values. These frequencies correspond to an integer number of points so the sinusoidal command may be defined (see PiMikroMove section). The tests carried out are shown below.

Amplitude 5 μm

The optical fiber is pre-tensioned to the value of 1000 $\mu\varepsilon$ by using the micropositioner. The Bragg wavelength in the static condition is $\lambda_{B_0} = 1565.96\,nm$. The PZT stage was controlled with a sinusoidal command with an amplitude of 5 μm. The frequency of the excitation signal is kept for 3.2 s for all tests.

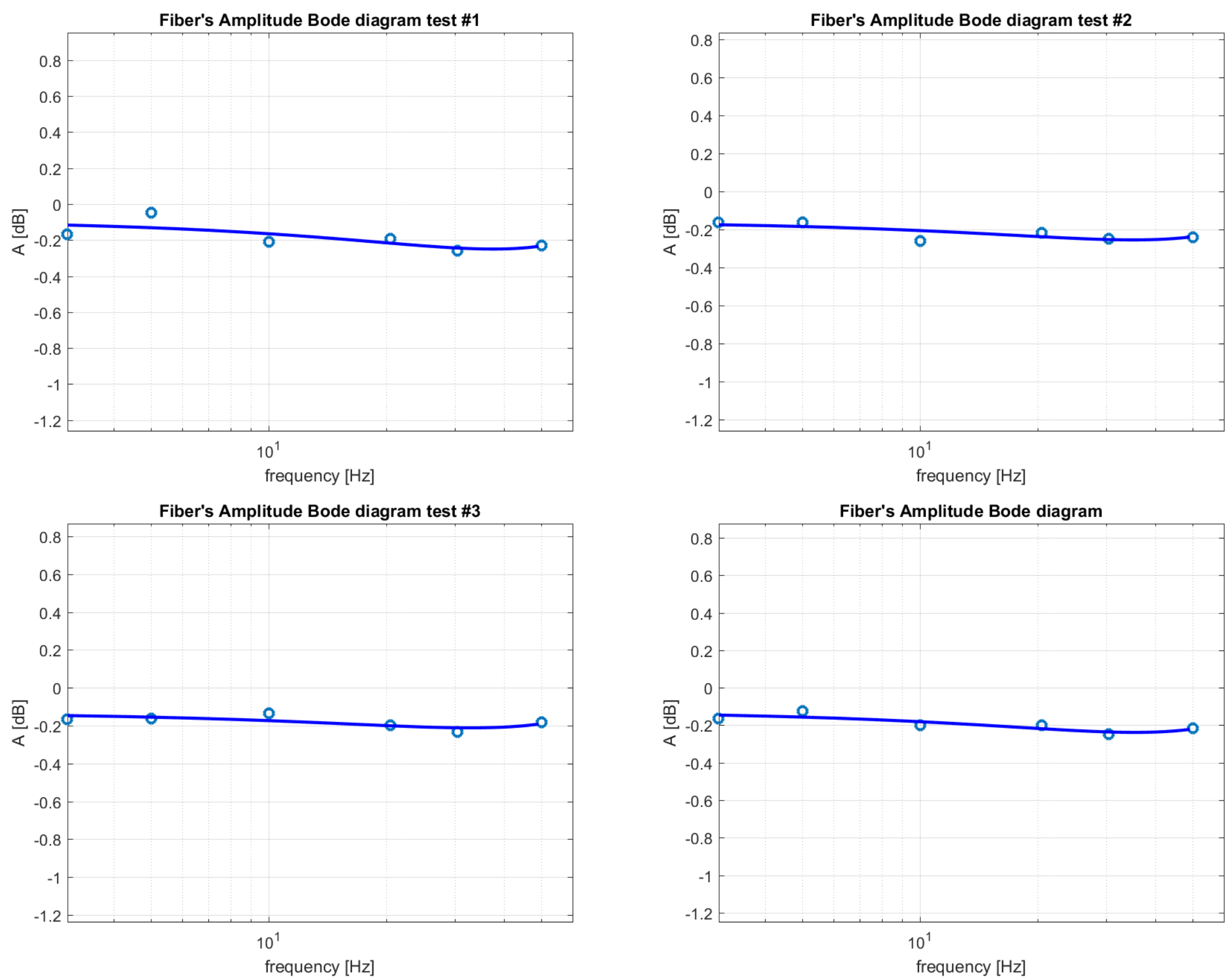

Figure 6.3: Bode diagrams at low frequency and amplitude of 5 μm

With an amplitude of 5 μm, approximately 50 $\mu\varepsilon$ (microstrains) are obtained. The amplitude of the FBG response has no significant variations at low frequency. Analyzing the frequency response, FBG has a linear behavior with an magnitude around 0 dB. This means that it responds with about the same amplitude of the piezo microstrains (4.3). The variations, that can be seen, between the three tests are negligible. They are due to measurement uncertainties.

Amplitude 10 μm

The same frequencies were used for these tests (table 6.1). Fiber tension has not been changed. The sinusoidal command has an amplitude of $10\,\mu m$. The figure 6.4 shows the results.

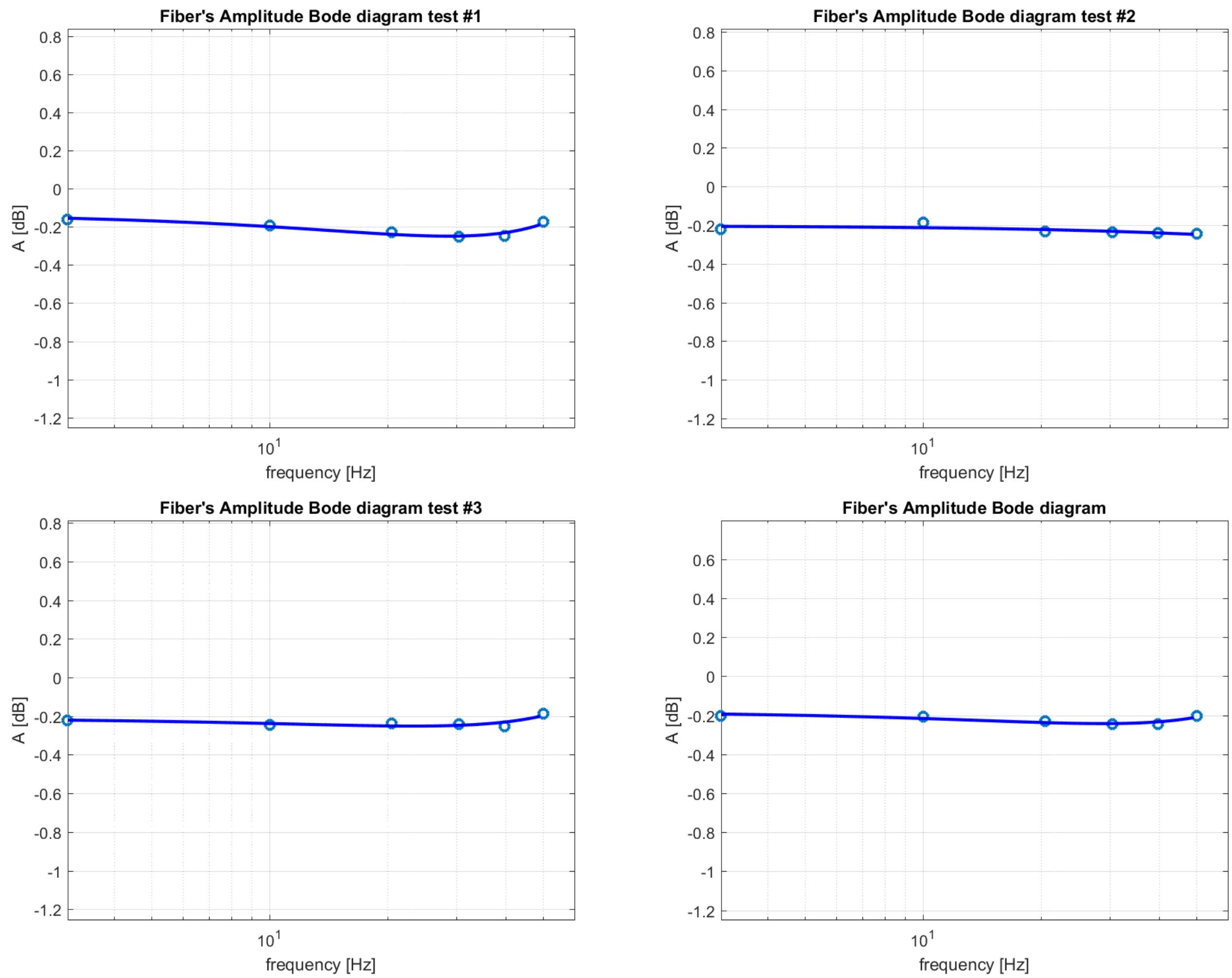

Figure 6.4: Bode diagrams at low frequency and amplitude of 10 μm

It is possible to observe that there are no significant variations when the amplitude is changed. At low frequency, doubling the input amplitude does not change the FBG response. By comparing the microstrains of the fiber, it is observed that by doubling the command amplitude, the microstrains are doubled. This is shown in the figure where the graphs of the fiber microstrain are plotted. In particular, both graphs were obtained for the frequency tests of $10\,Hz$.

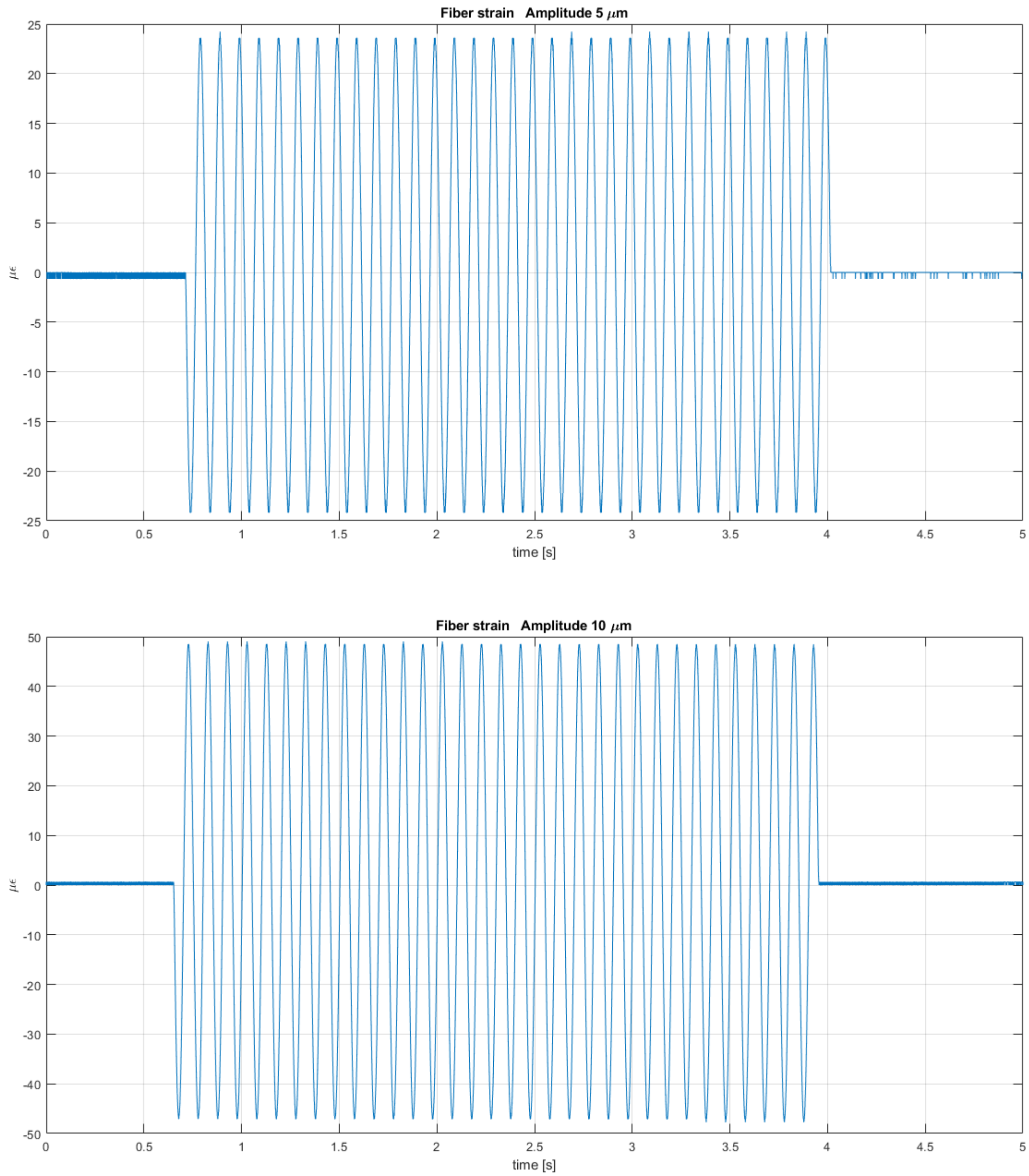

Figure 6.5: Microstrain ($\mu\varepsilon$) of optical fiber.

Complete test with amplitude 2 μm

After the low-frequency tests, a complete test was carried out with a command amplitude of 2 μm and with the frequencies shown in table 6.2. The optical fiber is pre-tensioned to the value of 1000 $\mu\varepsilon$.

3,0517	5	10	25	50	100	148,81	201,61	250

Table 6.2: Frequencies used in the complete tests

A single measurement was carried out for each frequency. In fact, as seen in previous tests, there were no significant changes in measurements in several consecutive tests for each frequency. For this reason only one bode diagram has been plotted. The figure 6.6 shows the results.

At low frequencies, upto approximately 100 Hz, the response is linear. As the input frequency increases, the response of the FBG sensor is amplified. Already at a frequency of 250 Hz amplification is important (fig 6.6). This can be explained by the phenomenon of resonance with standing waves that propagate along the fiber. So, we checked whether the optical fiber behaved like a vibrating cord fixed at both ends. In the next paragraph, the calculations carried out are detailed.

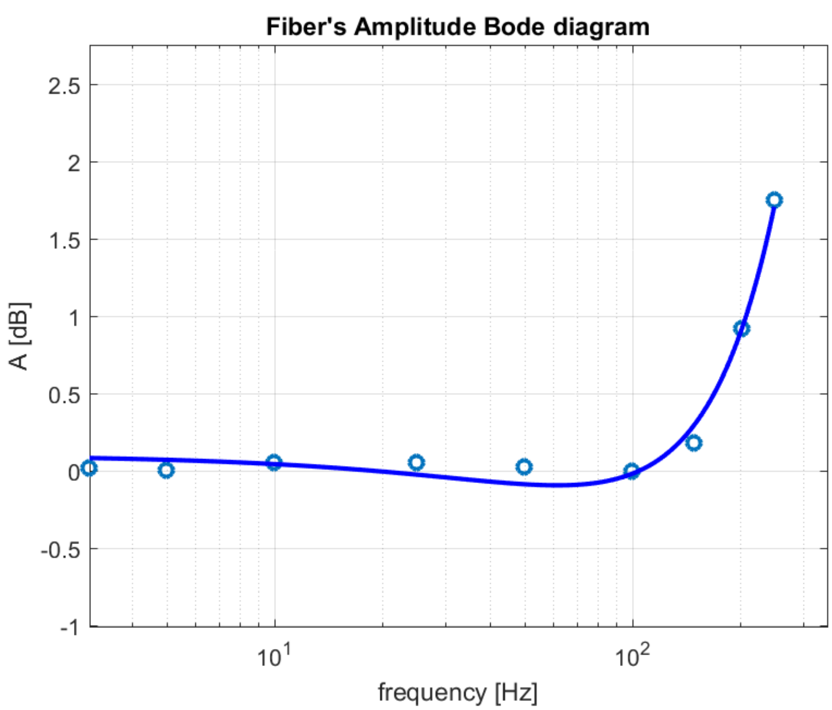

Figure 6.6: Test Bode diagram

6.1.1 Theory of vibrating string

The periodic perturbation induced by the PZT actuator causes standing waves to propagate along the optical fiber. The speed of the pulse through the medium, in this case the optical fiber, is a function of the properties of the optical fiber. Specifically, it is a function of the linear density and of the tension as shown by the following equation:

$$v = \sqrt{\frac{T}{\mu}} \tag{6.1}$$

where v $(m \cdot s^{-1})$ is the pulse speed, T (N) the tension in the string, and $\mu(kg \cdot m^{-1})$ the linear density of the string.

The transverse mechanical wave that travels along the string towards a fixed end will be reflected in the opposite direction. When a string is fixed at both ends, two waves travelling in opposite directions simply bounce back and forth between the ends. A form of the stationary wave equation can be defined as:

$$y = 2y_m sin\left(\frac{n\pi}{L}x\right) cos\left(\frac{n\pi v}{L}t + \alpha\right) \tag{6.2}$$

There are an infinite number of possible periodic motions, depending on the value of the integer n [10]. The frequencies are restricted to the values given by

$$f = \frac{nv}{2L} = \frac{n}{2L}\sqrt{\frac{T}{\mu}} \tag{6.3}$$

The simplest vibrational mode is for $n = 1$, where, the so-called "fundamental" frequency, is given by

$$f_0 = \frac{1}{2L}\sqrt{\frac{T}{\mu}} \tag{6.4}$$

In order to verify if the optical fiber had a behaviour described by the theory of the vibrating string, the natural frequency (also called fundamental) has been experimentally calculated and compared with the theoretical value.

6.1.1.1 Calculation of the natural frequency of the optical fiber

The optical fiber is fixed at both ends (fig 4.17) with $L = 0.1$ m. In these tests the PZT actuator is not used. The following data were used for the theoretical calculation of the natural frequency:

- $\Phi = 155$ μm diameter of optical fiber

- $A = 1.887 \cdot 10^{-8}\ m^2$ optical fiber section
- $E = 20\ GPa$ Young's module

The optical fiber tension has been calculated from the following relation:

$$T = \varepsilon \cdot A \cdot E \tag{6.5}$$

where ε are the microstrains. The SmartSoft software (see par. 5.2) can be used to display the value of the microstrains detected by the FBG sensor. Using the micropositioner, the fiber has been tensioned to the desired value. So the natural frequency was calculated for three different values of microstrains.

Results for $1000\ \mu\varepsilon$

The value of $1000\ \mu\varepsilon$ is the standard pretensioning used for the tests described in the section 6.1. Using equation 6.5, the tension is $T = 0.3774\,N$. With this tension value the theoretical natural frequency is $f_0 = 1565.42\,Hz$.

The experimental value was obtained from the measurements carried out by the SmartScan interrogator. The optical fiber was plucked at the midpoint and left to vibrate. Using the script matlab Post_processing_3_1 (see par. 5.3), the microstrain curve was plotted (fig 6.7). From the graph the time (Δt) between two consecutive peaks of the oscillation was been measured.

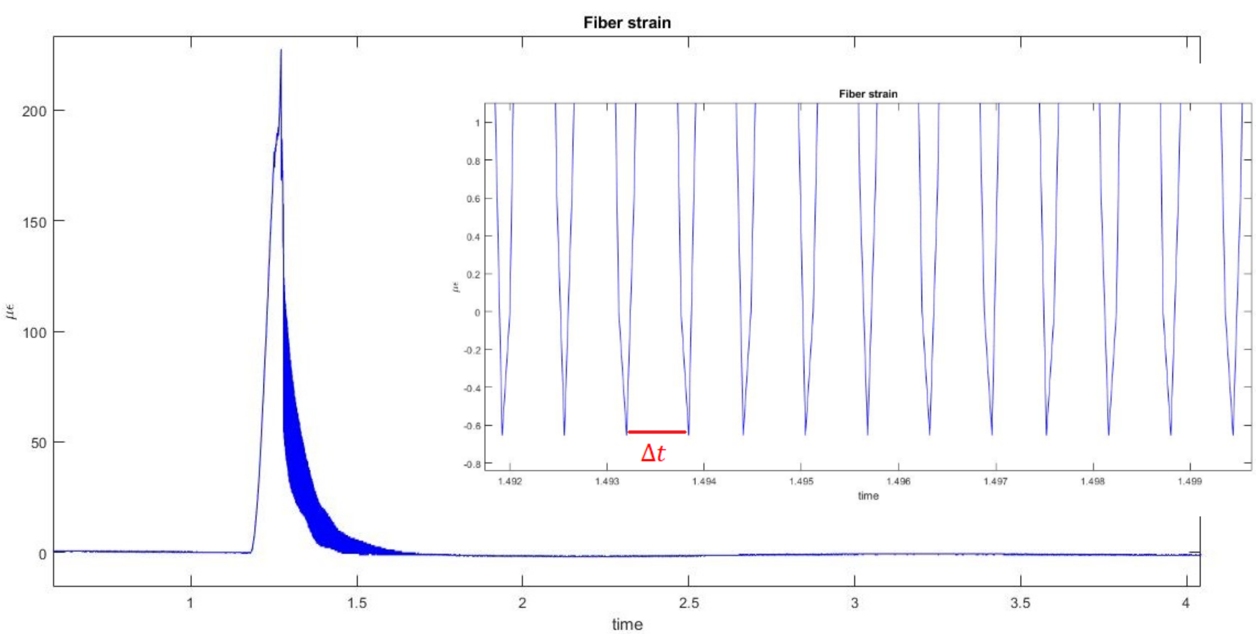

Figure 6.7: Microstrain plot: free oscillation of the optical fiber.

The natural frequency therefore resulted to be:

$$\frac{1}{\Delta t} = 1562.5\, Hz \tag{6.6}$$

Results for $500\,\mu\varepsilon$

According to equation 6.5 and 6.4, if the microstrains decrease, the tension and therefore the natural frequency decrease. Following the same procedure described above, the following results are obtained:

- $T = 0.1887\, N$
- $f_0 = 1106.9\, Hz$ theoretical value
- $f_0 = 1250\, Hz$ experimentally measured value.

The natural frequency also depends on the length L. If the free length increases, the frequency f_0 decreases according to the relation 6.4. To verify this experimentally, an optical fiber was glued to the maximum length available on the breadboard (fig. 6.8).

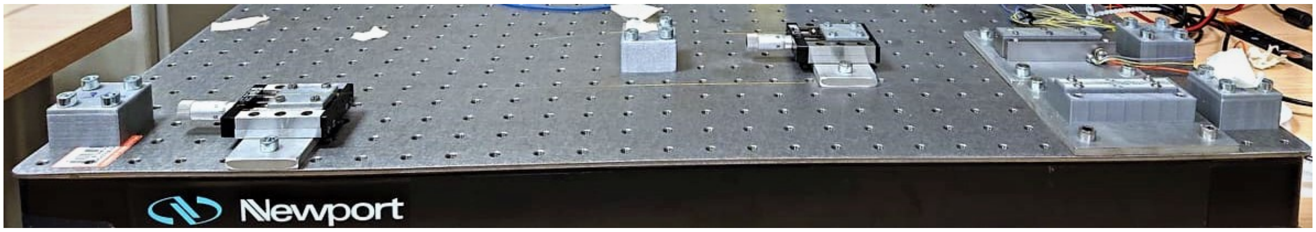

Figure 6.8: Optical fiber glued to the maximum available length

The gluing distance is $L = 0.45\ m$. With this new layout, the same tests were performed at 1000 $\mu\varepsilon$ and 500 $\mu\varepsilon$. The results are shown in the following table.

	T [N]	f_0 theorical [Hz]	f_0 misured [Hz]
L = 0.1 m			
500 $\mu\varepsilon$	0,1887	1106,9	1250
1000 $\mu\varepsilon$	0,3774	1565,45	1562,5
L = 0.45 m			
500 $\mu\varepsilon$	0,1887	245,98	297
1000 $\mu\varepsilon$	0,3774	347,88	357,1

Table 6.3: Test results about the natural frequency of the optical fiber

The frequencies measured experimentally are very close to the theoretical value. Particularly at higher tension, the measured values are even more accurate.

6.1.2 Tests with tension variation

The next dynamic analysis tests were carried out by varying the tensioning. The tests were performed on the optical fiber glued at $L = 0.1\ m$. Three different pretensions were used: 500 $\mu\varepsilon$, 1000 $\mu\varepsilon$, 2000 $\mu\varepsilon$. Not having the actual values of the tension, we refer to the microstrains. They are directly proportional to the tension value according to the relation 6.5. The amplitude command was 2 μm and three input frequency values were used: 148.1 Hz, 201.61 Hz, 250 Hz. After pretensioning the fiber, four consecutive tests were carried out for each frequency and the average value of the amplitude (dB) was calculated.

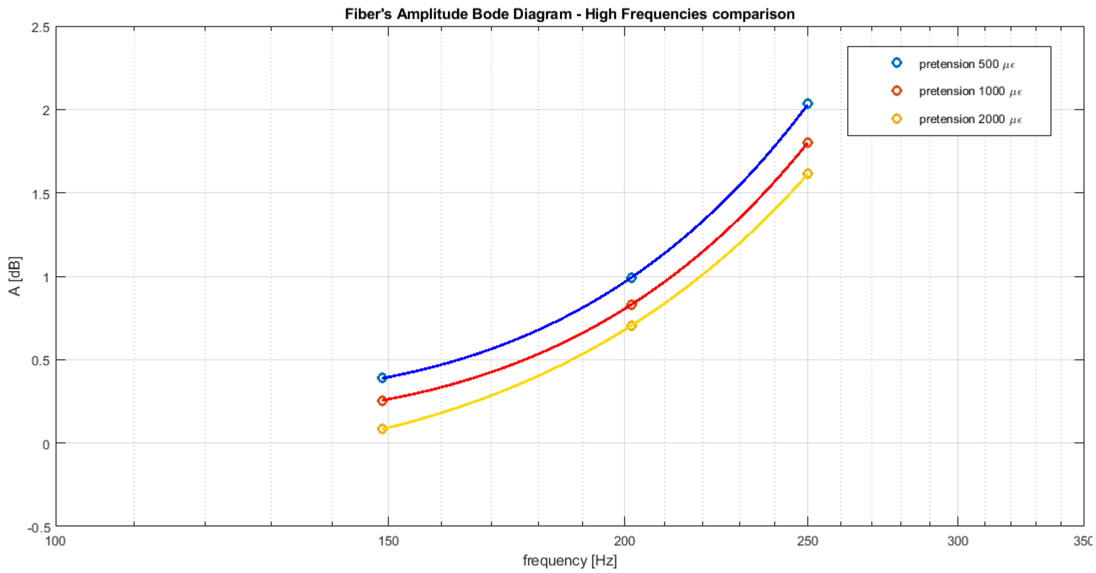

Figure 6.9: Comparison of the frequency response of three different pretensions

The figure 6.9 shows the results of the tests. If the natural frequency f_0 increases, the oscillations will be less amplified by the effect of resonance. From the results of the tests, in fact, as the tension increases, there is a higher natural frequency and the peak amplification is lower. Therefore, at the same excitation frequency, with lower tensions there is a higher amplification. So, the optical fiber probably has a behaviour similar to a vibrating string. However, the oscillatory phenomena that occur during a dynamic test are very difficult to predict. Experimentally there are many boundary conditions that make it difficult to study the phenomenon.

6.2 Problems and limitations

During the tests, a number of problems were identified which caused measurement uncertainties. For some conditions these problems can be relatively overlooked while for others they become a serious limit. For some conditions, these problems can be relatively neglected while for others they become a real limit. At the end of all the tests, it was possible to identify the main problems that can become the subject of study in successive theses.The problems and limitations encountered will be illustrated and explained below.

The first problem concerns the measurements performed by the SmartScan interrogator. The tests have shown that there are static fluctuations in the measurement (fig. 6.10). In the case of resting optical fibre, the interrogator records a fluctuation of about $\pm 0.6\ \mu\varepsilon$ (the microstrains are calculated from the wavelength recorded according to the relation 3.8).

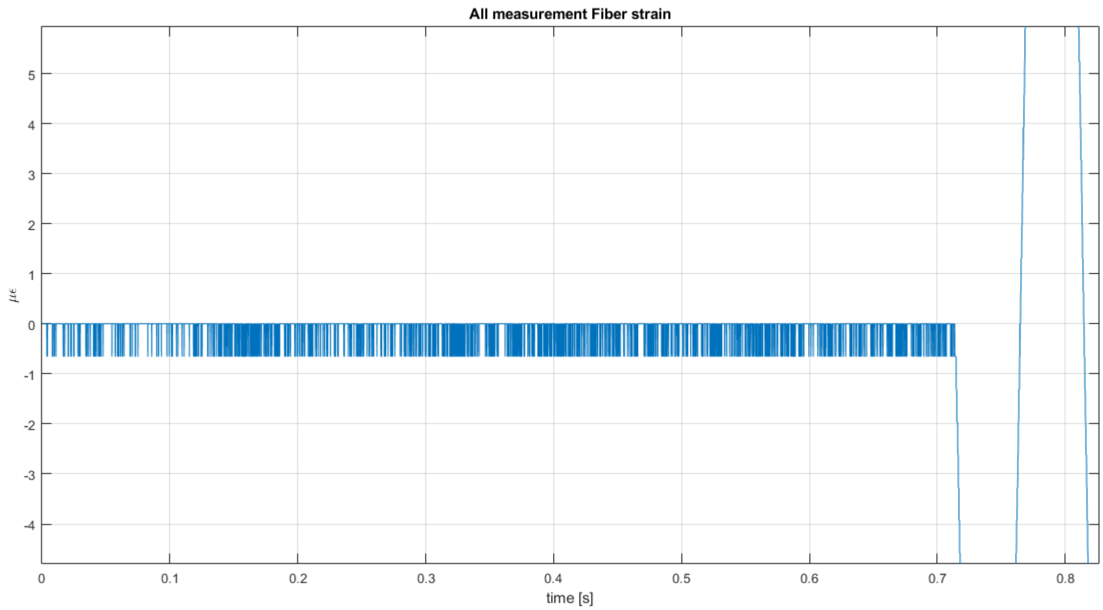

Figure 6.10: Static fluctuations in measurement

These random fluctuations affect the dynamic test by causing peaks in the wave amplitude as shown in the figure 6.11. The measurement can be influenced by these peaks in several cases which mainly concern the number of waves and the amplitude of the fiber response.

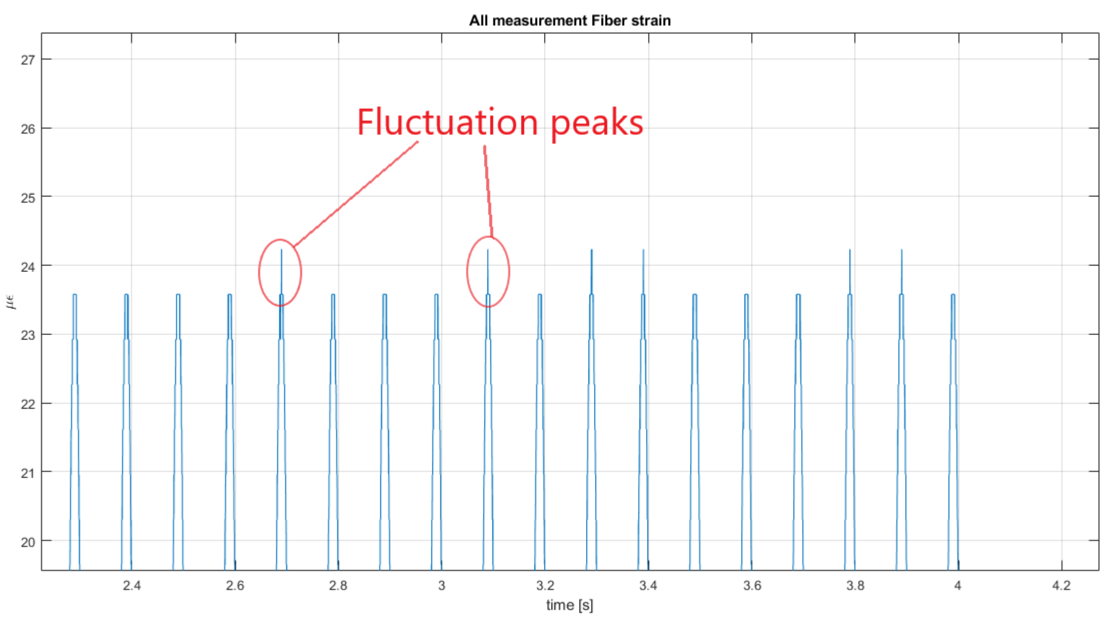

Figure 6.11: Fluctuation peaks in the measurement

The low frequency fiber response is characterized by fewer waves over the test duration time. Remember the magnitude (dB) is calculated on the averange value of the amplitudes ($\mu\varepsilon$). Therefore, if there are peaks in a few waves, they cannot be mitigated by the average. Moreover, they are absolutely random. In the tests where the command generated a fiber response with amplitudes greater than25 $\mu\varepsilon$, the fluctuation of $\pm 0.6\ \mu\varepsilon$ can be overlooked. In the case of optical fiber glued at 0.1 m, the sinusoidal command must have an amplitude of at least 2 μm. For smaller command amplitudes the effect of fluctuations becomes relevant.

With the fibre glued at 0.45 μm (fig. 6.8), a sinusoidal command with an amplitude of 2 μm is too small. In fact, the amplitude of the fiber response is less than 5 $\mu\varepsilon$. Therefore, the fluctuations on this measure become significant (fig. 6.12) and the measurement becomes unreliable.

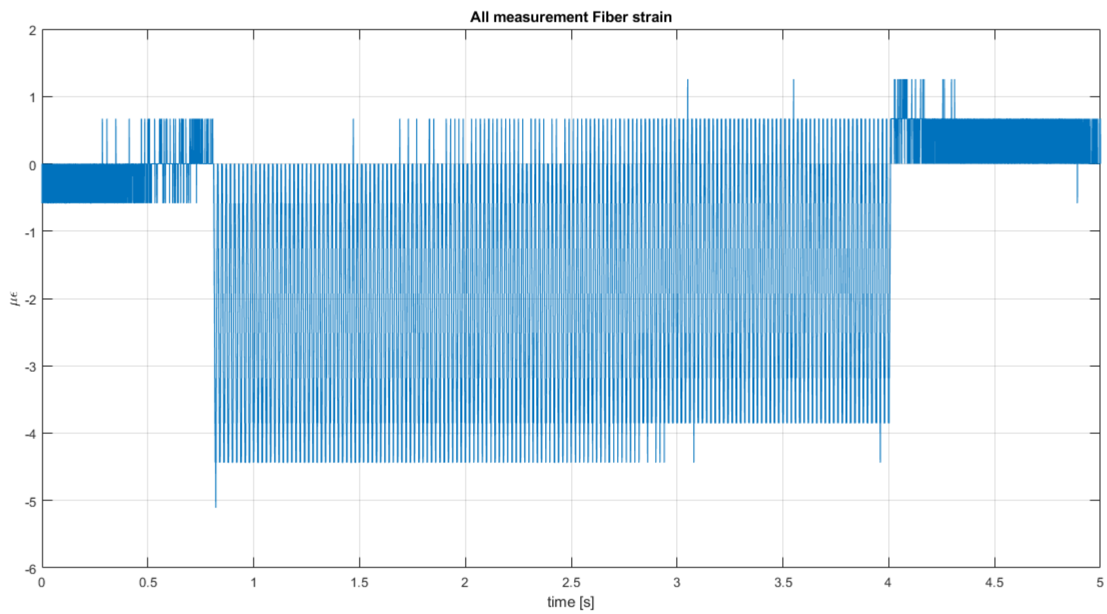

Figure 6.12: Test at frequency of $50 Hz$ and amplitude2 μm.

This means that it is necessary to give a sinusoidal command with high amplitude. But this is not possible when using the PZT actuator. The actuator has an attenuated response as the frequency increases (fig. 6.14). During the tests to obtain a constant amplitude at all frequencies, sinusoids (with *PI WaveGenerator tool*) were created with ever increasing amplitudes in order to obtain a movement of the piezo with the desired amplitude.

FREQUENCY (Hz)	COMMANDED AMPLITUDE (μm)	REAL AMPLITUDE (μm)	THEORETICAL AMPLITUDE (μm)
3,0517	2	2	2
5	2	2	2
10	2	2	2
25	2	2	2
50	2,3	2,01	2
100	3	1,98	2
148,81	4	1,99	2
201,61	5,9	2,01	2
250	8	1,97	2

Table 6.4: Table of command amplitudes

Referring to table 5.1, the second column shows the values used to create the wave in *PI Wave Generator Tool*, while the third column shows the amplitude measured in the graph of the actuator response (fig 6.13).

As the frequency increases, the attenuation is always greater as shown in the bode diagram in the figure 6.14.

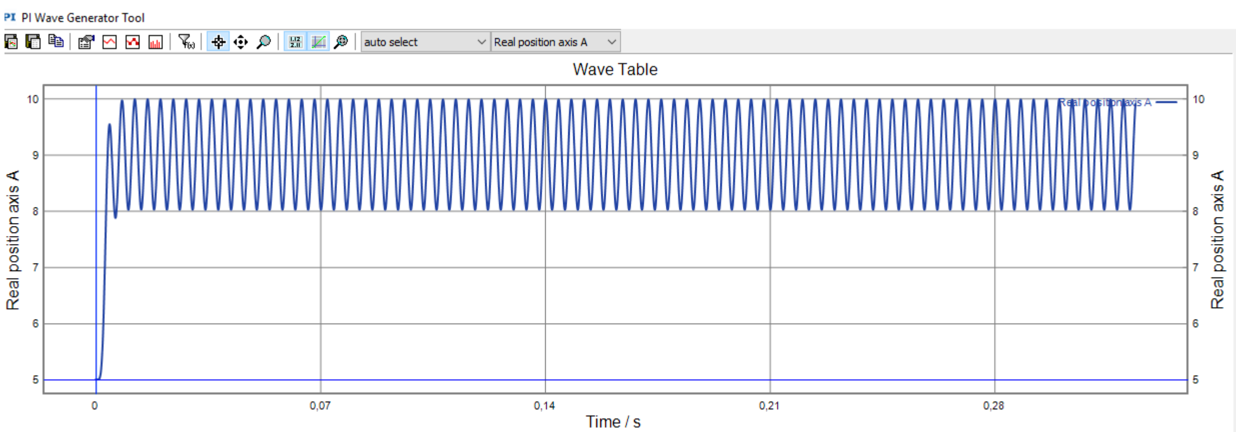

Figure 6.13: Graph of the PZT response with a sinusoidal command at a frequency of 250 $Hz$and an amplitude of 8 μm

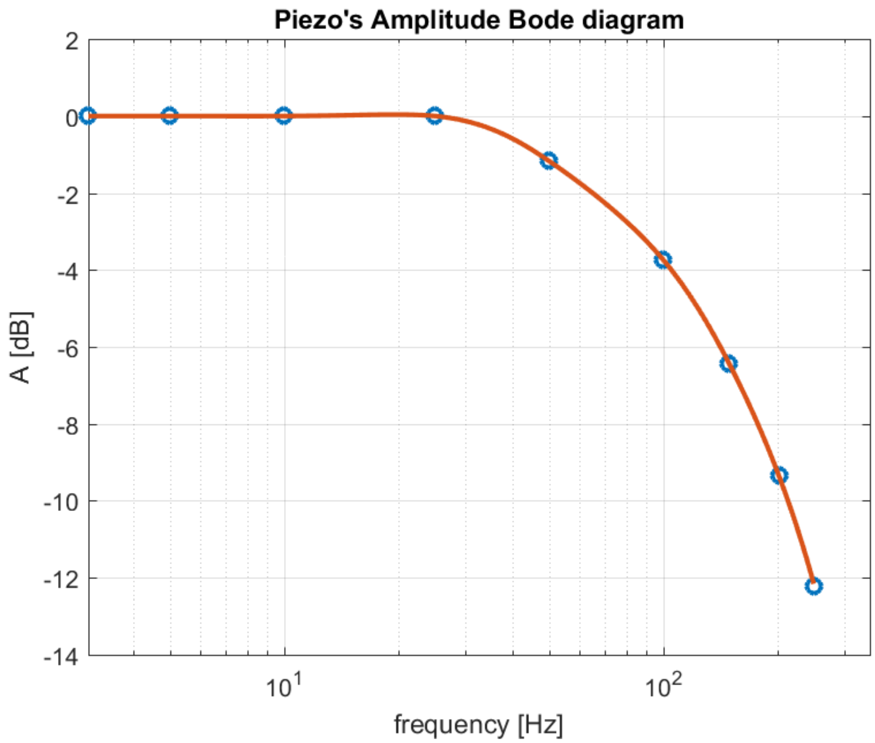

Figure 6.14: Bode diagram of PZT actuator

Considering the operating limits of the piezoelectric, it was not possible to carry out tests at high frequency (greater than 300 Hz) with amplitude greater than 2 μm. To obtain higher amplitudes at high frequency it means to control the piezo with high voltages and which would limit its working life and the possibility of breakdown.

6.3 Test with accelerometer

This section describes the use of an accelerometer to validate the command provided by the piezoelectric actuator. The calculation of the magnitude (dB) of the optical fibre was carried out using as input (equation 6.2) the data provided by the *PIMikroMove* software. Then, to ensure that the data provided were correct, they were compared with the data provided by an accelerometer. In particular, the recorded frequency was verified.

The model of accelerometer used is the ADXL345. The ADXL345 is a small, ultralow power, 3-axis MEMS accelerometer with measurement of upto $\pm 16g$. Digital output data is formatted as 16-bit twos complement and is accessible through either a *SPI* (3- or 4-wire) or I^2C digital interface. It measures both dynamic acceleration resulting from motion or shock and static acceleration, such as gravity. It supports output data rates ranging from 10 Hz to 3200 Hz.

The boards (fig. 6.15) for these modules feature on-board 3.3 V voltage regulation and level shifting which makes them simple to interface with 5 V microcontrollers such as the Arduino.

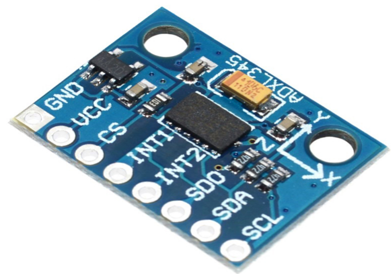

Figure 6.15: Accelerometer module ADXL345

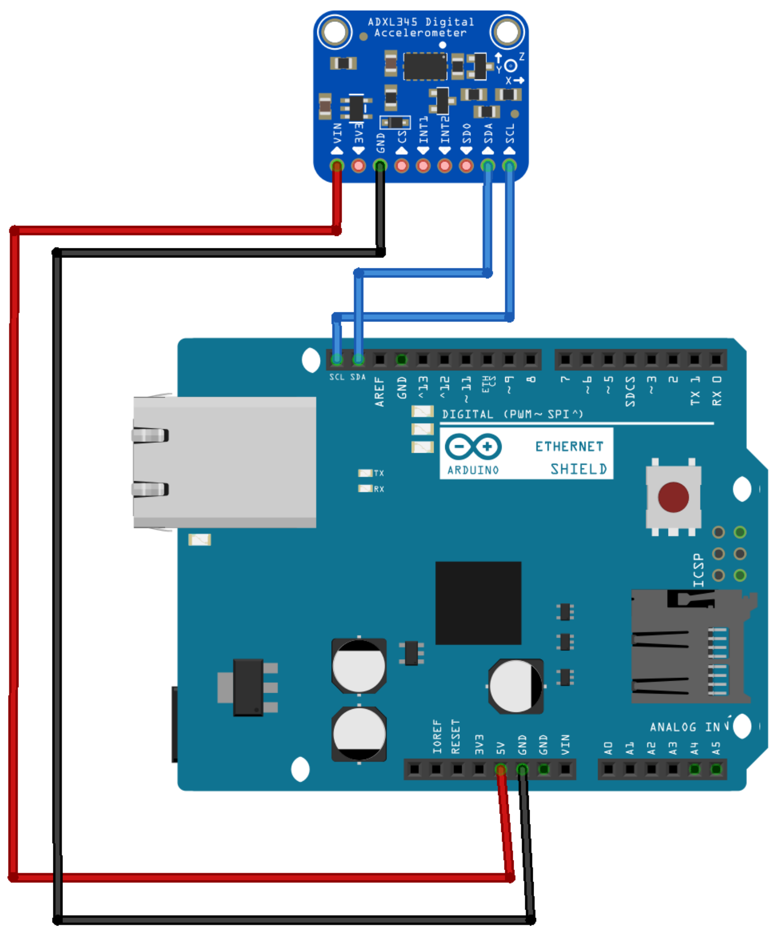

Figure 6.16: Wiring diagram between ADXL345 and Arduino

The ADXL345 has been connected to Arduino Uno via I^2C serial communication. In this mode, it require a simple 2-wire connection (i.e the pin *SDA* and *SCL*), as shown in figure 6.16. The power supply is 5 V. An Ethernet Shield with micro SD has been used for data storage.

The *Arduino* software has been used for the part of the code. For this accelerometer model there are libraries with codes already implemented. A part of the code has been added to allow the data to be stored on the SD memory. In particular, the program opens a file on the SD and saves on it the measurements of the ADXL345 accelerometer. Data rate of 3200 Hz was used. In the file, the acceleration values along the x-axis (displacement axis of the piezo actuator) and the time are saved. For higher sampling rates and data storage, the time value is saved one every twenty. In the post-processing they will be then interpolated.

For the post-processing of the data has been written a matlab script, *Lettura_accelerometro*. This script allows to import the data of the file present on the SD and, after the interpolation of the times, it plots the graph of the accelerations.

6.3.1 CAD assembly design

To fix the ADXL345 board on the PZT actuator, a plate has been designed and printed in PLA. The plate size is $73.5 \times 16 \times 3\ mm$. There are four M 2.5 holes for mounting the plate to the piezo. Two hexagonal seats have been made to enable to insert the nuts and fix the ADXL345 with the screws. To avoid an inclination of the board caused by the contact between the solder pins and the plate, a rectangular groove has been made (fig. 6.17). The cad assembly is shown in the figure 6.18.

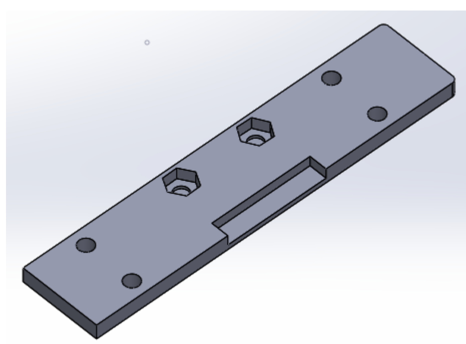

Figure 6.17: Plate for mounting the ADXL345 on the piezo actuator

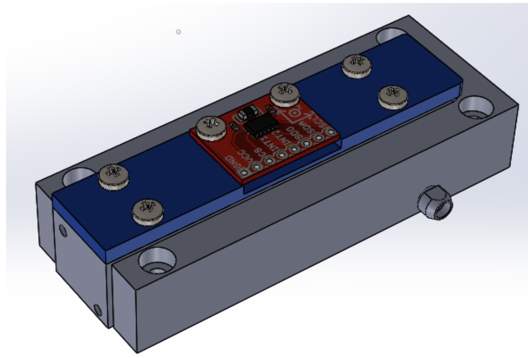

Figure 6.18: Cad assembly

6.3.2 Measurements

The accelerometer is used to validate the dynamic response of the piezo and related data obtained from the PIMikroMove software. The piezo is moved with a sinusoidal command. The aim is to measure the frequency of the recorded acceleration and to compare it with the frequency of the displacement recorded by the *data recorder* of the modular piezo controller (section 4.3.1). The layout on the test bench is shown in the figure 6.19.

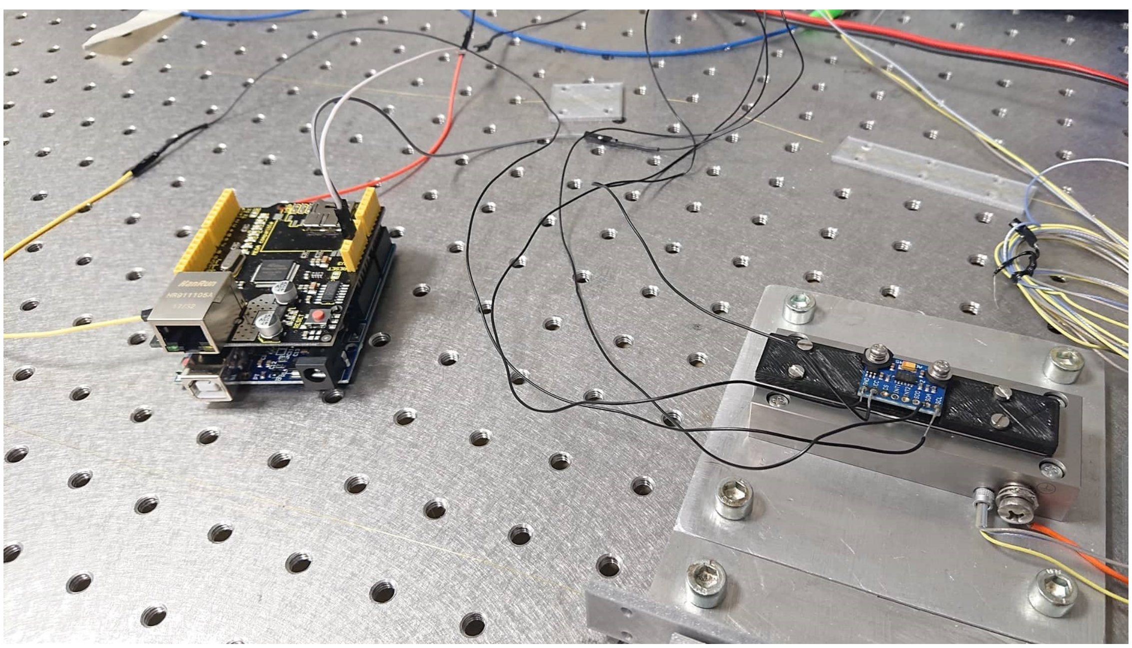

Figure 6.19: Layout for the test of the ADXL345

In our case where the vibration is represented by a simple harmonic motion, of amplitude A (μm) and pulsation ω (rad/s), the acceleration is expressed through the relation:

$$\ddot{x}(t) = -\omega^2 A sin(\omega t)$$

where the frequency is $f = \frac{\omega}{2\pi}$. The amplitude of the acceleration is directly proportional to ω. Therefore, for high frequencies the measurement is more easily appreciable (in amplitude).

The tests were carried out by creating the sinusoidal command using the *PI Wave Generator Tool* and recording the accelerations during the motion of the piezo actuator.

The first test was performed at 25 Hz with amplitude 30 μm. In this case the frequency is too low and the measurement is dirty by the noise in the accelerometer.

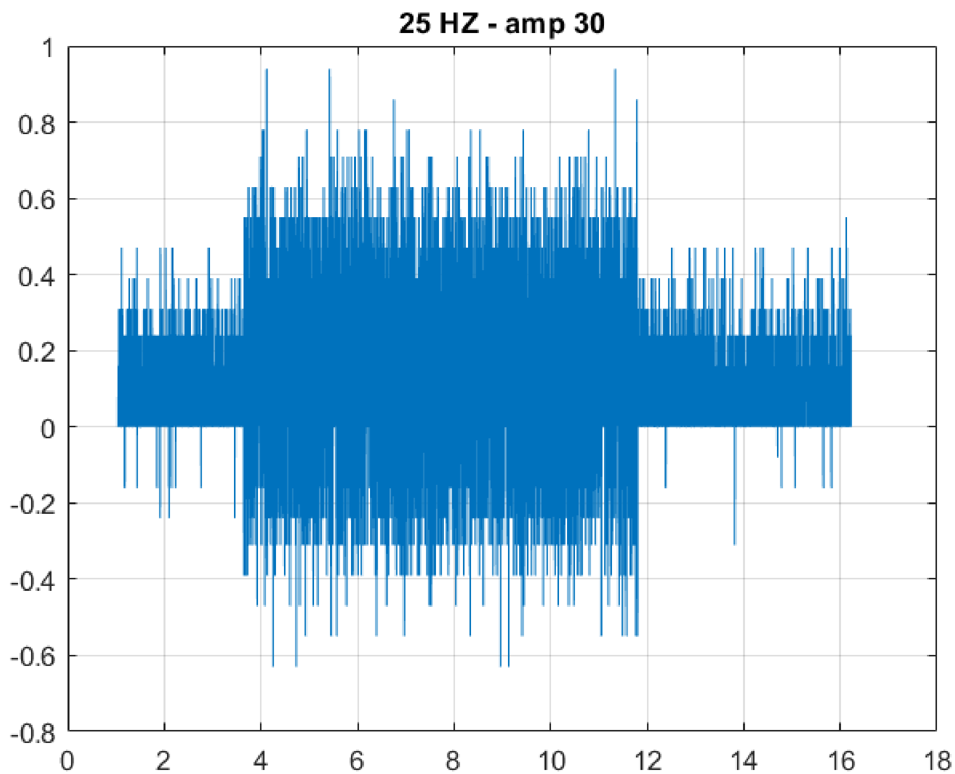

Figure 6.20: Acceleration measurement at 25 Hz

With a command of amplitude and frequency of 35 μm and 40 Hz (exact value40.98 Hz) respectively, the amplitude of the acceleration is appreciable. Two peaks were chosen and their distance in time was measured and then the frequency is calculated. The result of the acceleration frequency is 39.1 Hz.

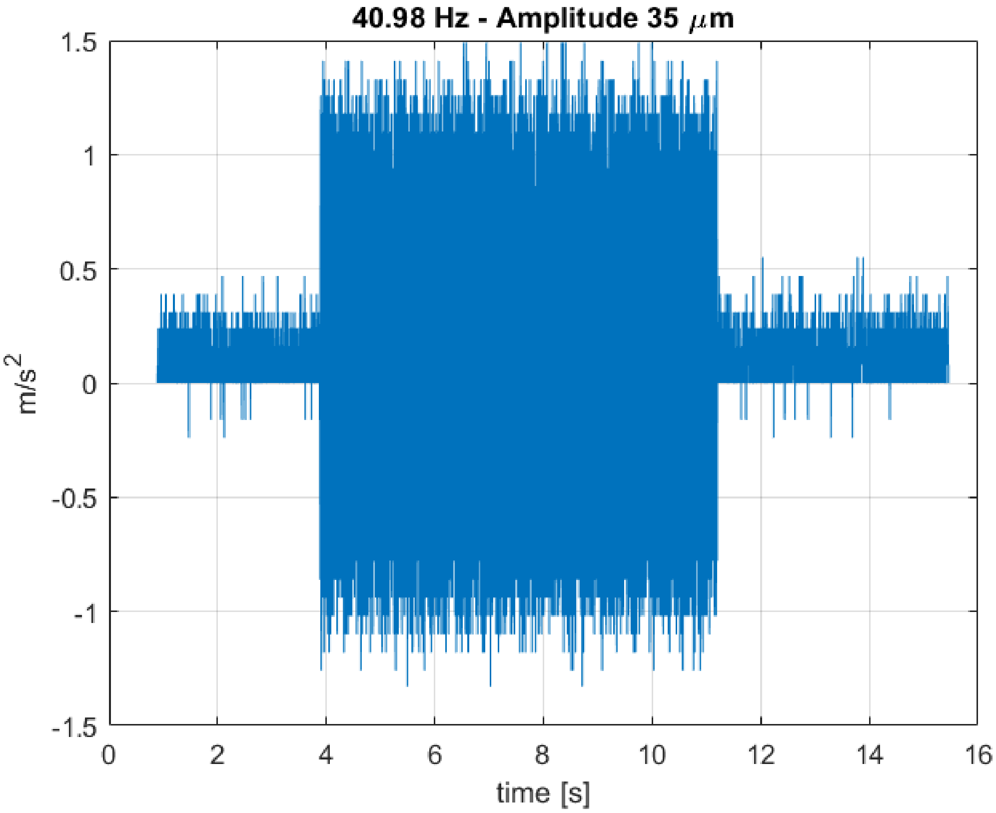

Figure 6.21: Acceleration measurement at 40.98 Hz

The test was repeated for a frequency of 50 Hz, so you can have a measurement that is less affected by noise. In this case, three different pairs of peaks were found and the frequencies were calculated. The measured frequencies are equal to 52 Hz, 51 Hz and 51 Hz.

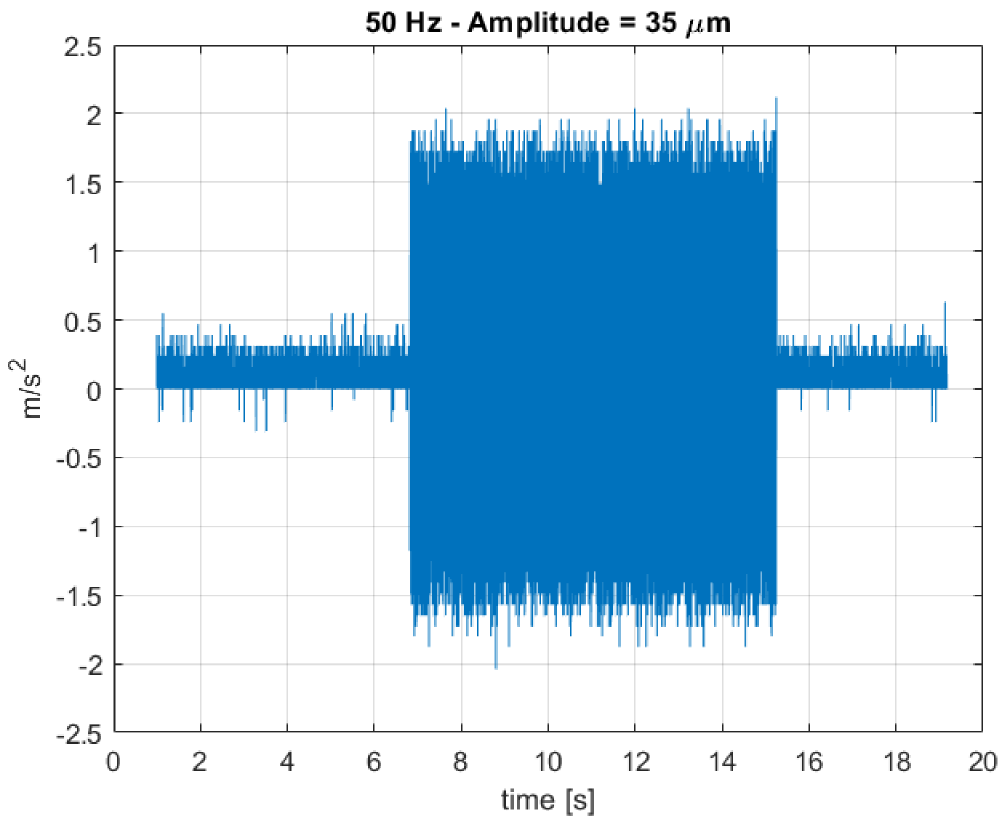

Figure 6.22: Acceleration measurement at 50 Hz

From the results obtained (table 6.5), considering the inaccuracies due to the boundary conditions of the whole experimental system, we can conclude that the piezo vibration frequency is correct. This means that the data recorded by modular piezo controller is correct and therefore the optical fiber vibrates with the exact command desired. In particular, the fiber amplification values are not due to wrong data related to the PZT actuator.

FREQUENCY PZT ACTUATOR [Hz]	FREQUENCY ADXL345 [Hz]
40	39,1
50	52
	51
	51

Table 6.5: Table of test results with the ADXL345 accelerometer

Chapter 7

Conclusions and future works

The research activity carried out in this thesis has been aimed at an initial dynamic analysis of the optical fiber. The development of the test bench was based on the conclusions of the previous work of the PHOTONEXT research team. In particular, the analysis of the dynamic behaviour of the FBG sensor was carried out using a similar test layout and the same method of fixing the optical fiber. The fixing method used was gluing. The test layout has been modified in order to adapt it to the new hardware needed for dynamic tests.

The device provided to induce a vibrational dynamic to the fiber was a piezoelectric actuator. This device, as written in section 6.2, has limitations in order to fully evaluate the dynamic behavior of the optical fiber, in particular, if it is used with this layout (fig. 4.1).

The results discussed in the previous chapter showed that the fiber behaves like a vibrating string. In the initial planning phase, it was not expected that the optical fibre could have such behaviour. This problem could be resolved by placing the optical fiber differently. To continue this research work about the frequency response of the FBG, it would be necessary to modify the test setup. By changing the fiber layout, it is expected that the dynamic behaviour will be better characterised.

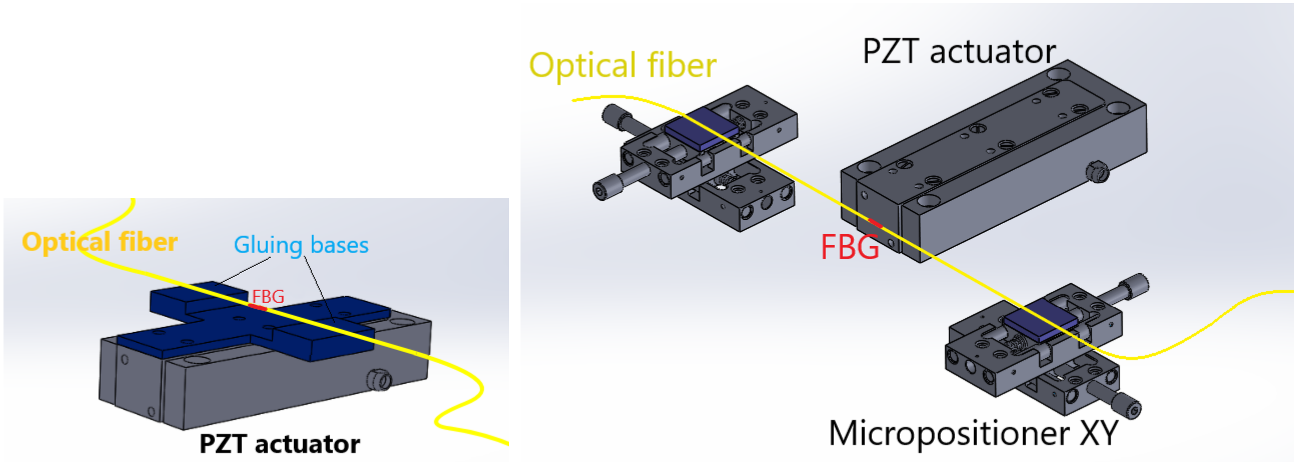

Figure 7.1: The new possible test-layout

The figure 7.1 shows two new possible setups for dynamic tests of the FBG sensor. These new configurations, always, require the use of the PZT actuator. If you continue to use this device in future work, it will be necessary to optimize the matlab programs for post processing. The aim will be to reduce the work of to the user as much as possible, so as to reduce the processing time of the data. In addition, it would be necessary to implement filters for the filtering of signals so as to minimize the influence of noise.

Another possibility is to use a different vibration generator such as a mechanical shaker, a loudspeaker or an ultrasonic signal generator.

All these new possible dynamic tests aim to have a clear understanding of the vibration behaviour of the FBG sensor. In this way, a package can be developed for application of the sensor on components subjected to high vibration stress. In addition, a package can be developed for application of the sensor on components subjected to high vibration loads. It will be important to understand how to integrate the sensor into different components in order to have a sensor system that allows you to perform the desired measurements.

Bibliography

[1] Gioele Baima. Design and development of a test bench for frequency analysis of fbgs optic sensors for prognostic techniques for aerospace applications. Master's thesis, Politecnico di Torino, 2019.

[2] Tandon Poonam Bhattacharya, D.K. Engineering physics: 5.7.5 illumination and image transfer, 2015.

[3] Jr. Eric Udd, William B. Spillman. *Fiber Optic Sensors: An Introduction for Engineers and Scientists*. 2011.

[4] Murata Hiroshi. *Handbook of Optical Fibers and Cables Second Edition*. 1996.

[5] R.P. Khare. *Fiber-Optics-Optoelectronics*. Oxford University Press, 2004.

[6] L.C. Klein. Piezoelectrics, 1988.

[7] Bessie A. Ribeiro Marcelo M. Werneck, Regina C. S. B. Allil and Fabio V. B. de NazarÃ©. A guide to fiber bragg grating sensors. Technical report.

[8] Springfield Technical Community College Massa, Nicholas M. *Fundamentals of Photonics*. 2008.

[9] Micron Optics. Optical fiber sensors guide fundamentals & applications. *www.micronoptics.com*.

[10] Robert H. Randall. 7.9 interpretation of the stationary wave equation, 2005.

[11] Enrico Tessadori. Misure di deformazione e temperatura mediante sensori a fibra ottica: tecniche di disaccoppiamento del segnale. Master's thesis, Politecnico di Milano, 2011.

[12] Perrone Guido Tosi, Daniele. Fiber-optic sensors for biomedical applications, 2018.

[13] W. H. Glenn W. W. Morey, G. Meltz. Fiber optic bragg grating sensors. 1989.